AD-A176 318 A PRELIMINARY INVESTIGATION OF NONLINEAR OPTOACOUSTIC SOUND GENERATION PROCESSES(U) TEXAS UNIV AT AUSTIN APPLIED RESEARCH LABS N P CHOTIROS 12 AUG 86 1/1

UNCLASSIFIED ARL-TR-86-11 N00014-86-K-0176 F/G 20/1 NL

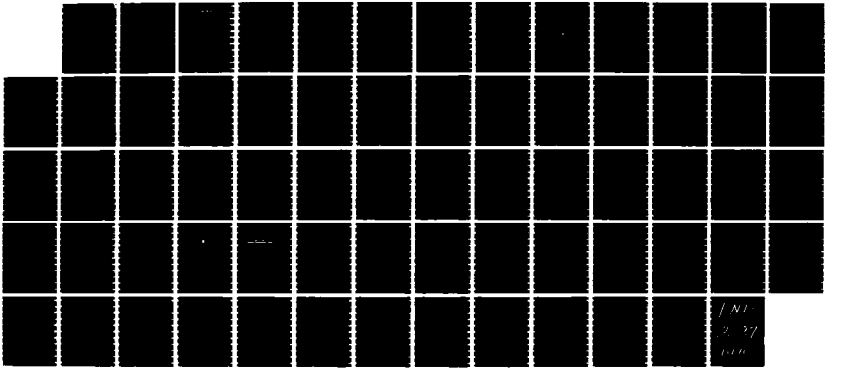

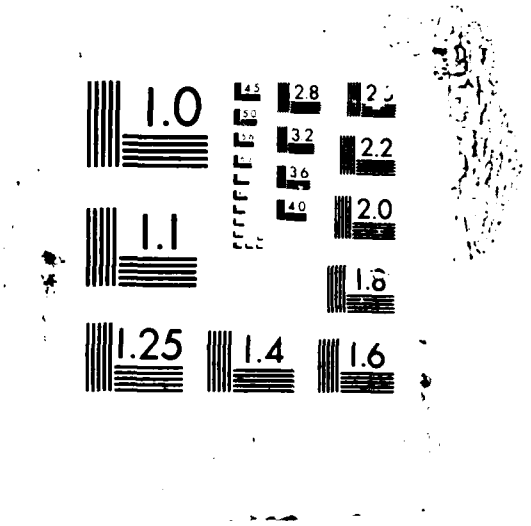
1.0
1.1
1.25
1.4
1.6
1.8
2.0
2.2
2.8
3.2
3.6
4.0

ARL-TR-86-11

Copy No. 7

A PRELIMINARY INVESTIGATION OF NONLINEAR OPTOACOUSTIC SOUND GENERATION AND LOSS

Nicholas P. Chotiros

APPLIED RESEARCH LABORATORIES
THE UNIVERSITY OF TEXAS AT AUSTIN
POST OFFICE BOX 8029 AUSTIN, TEXAS 78713-8029

2 August 1986

Technical Report

UNCLASSIFIED

SECURITY CLASSIFICATION OF THIS PAGE *(When Date Entered)*

(12)

REPORT DOCUMENTATION PAGE	READ INSTRUCTIONS BEFORE COMPLETING FORM
1. REPORT NUMBER	2. GOVT ACCESSION NO. AD-A176 318 / 3. RECIPIENT'S CATALOG NUMBER
4. TITLE *(and Subtitle)* A PRELIMINARY INVESTIGATION OF NON' NEAR OPTOACOUSTIC SOUND GENERATION PROCESSES	5. TYPE OF REPORT & PERIOD COVERED technical report
	6. PERFORMING ORG. REPORT NUMBER ARL-TR-86-11
7. AUTHOR(s) Nicholas P. Chotiros	8. CONTRACT OR GRANT NUMBER(s) N00014-86-K-0176
9. PERFORMING ORGANIZATION NAME AND ADDRESS Applied Research Laboratories The University of Texas at Austin Austin, Texas 78713-8029	10. PROGRAM ELEMENT, PROJECT, TASK AREA & WORK UNIT NUMBERS
11. CONTROLLING OFFICE NAME AND ADDRESS Office of Naval Research Department of the Navy Arlington, Virginia 22217	12. REPORT DATE 12 August 1986
	13. NUMBER OF PAGES 66
14. MONITORING AGENCY NAME & ADDRESS*(if different from Controlling Office)*	15. SECURITY CLASS. *(of this report)* UNCLASSIFIED
	15a. DECLASSIFICATION/DOWNGRADING SCHEDULE

16. DISTRIBUTION STATEMENT *(of this Report)*

Approved for public release; distribution unlimited.

17. DISTRIBUTION STATEMENT *(of the abstract entered in Block 20, if different from Report)*

18. SUPPLEMENTARY NOTES

19. KEY WORDS *(Continue on reverse side if necessary and identify by block number)*

laser
optoacoustics

20 ABSTRACT *(Continue on reverse side if necessary and identify by block number)*

In the generic optoacoustic sound source, a laser beam is directed at the water surface to produce a controlled local reaction which, in turn, generates sound waves. The energy is delivered without physical contact. At low optical intensities, the reaction is a linear thermal expansion of the medium, but at high intensities, the reaction is nonlinear and more complicated. A simple blast model is used to predict the acoustic output of the high intensity reaction. The blast model is based on that of A. N. Pirri who successfully

DD FORM 1 JAN 73 1473 EDITION OF 1 NOV 65 IS OBSOLETE

UNCLASSIFIED

SECURITY CLASSIFICATION OF THIS PAGE*(When Date Entered)*

20. (cont'd)

used it to model the momentum transfer between a high power laser blast on the surface of a solid. The Pirri model is general enough to be adapted for laser induced blasts over water. The model predictions are compared with experimental results. The differences are discussed.

TABLE OF CONTENTS

LIST OF FIGURES

I. INTRODUCTION

Applied Research Laboratories, The University of Texas at Austin (ARL:UT), has been investigating both theoretically and experimentally the basic properties of thermoacoustic sources. The thermoacoustic process employs direct heating of the acoustic medium to produce a controlled local thermal expansion which, in turn, generates sound waves. The thermal energy is delivered by a laser beam to the water through the free surface without physical contact. The efficiency of the thermoacoustic conversion process is an important issue. An analysis was made of the upperbound and it was found to be constrained by the physical properties of the medium and the energy output of the thermal source.[1]

The thermoacoustic process is only one of several optoacoustic processes for converting optical energy into acoustic energy. It is often referred to as the linear process. It is linear in the sense that, over a large range of temperatures, the change in density of the water is linearly proportional to the optical energy input, at least for small input energy densities. The general concept is illustrated in Fig. 1. Other processes by which optical energy is converted to sound are grouped together under the title of nonlinear processes. The current knowledge regarding nonlinear processes was thoroughly reviewed by Lyamshev and Naugol'nikh.[2] Nonlinear processes, in general, have been found experimentally to be more efficient but they are not well understood.

The anatomy of the optoacoustic processes is illustrated in Fig. 2. The main processes include: weak and strong evaporation, optical breakdown of the vapor, and optical breakdown of the liquid. They are mainly governed by the intensity and energy density of the laser pulse. Evaporation processes are mainly governed by energy density. Weak evaporation refers to the evaporation of a thin surface layer of the liquid, while strong evaporation refers to explosive bubbling from the surface and from the interior of the liquid.

Evaporation processes can take place only when the energy absorbed is equal to or greater than the specific internal energy required for the phase change. The absorbed energy is directly governed by the delivered surface energy density and by the absorption coefficient. For 1.06 μm laser radiation, the absorption coefficient is

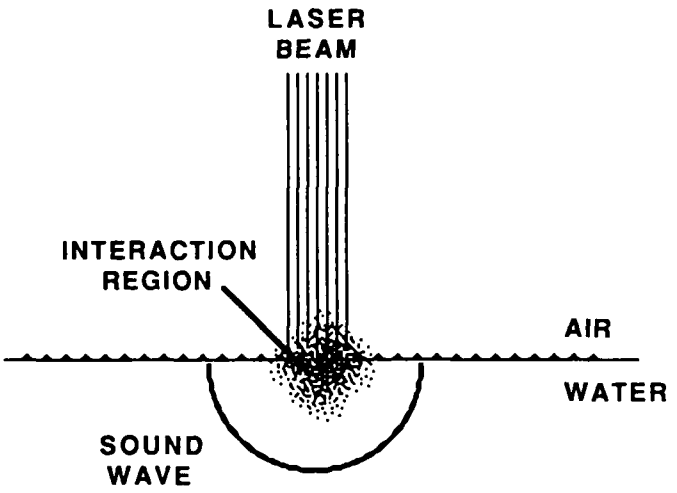

FIGURE 1
THE THERMOACOUSTIC CONCEPT

ARL:UT
AS-86-474
NPC - GA
1 - 9 - 86

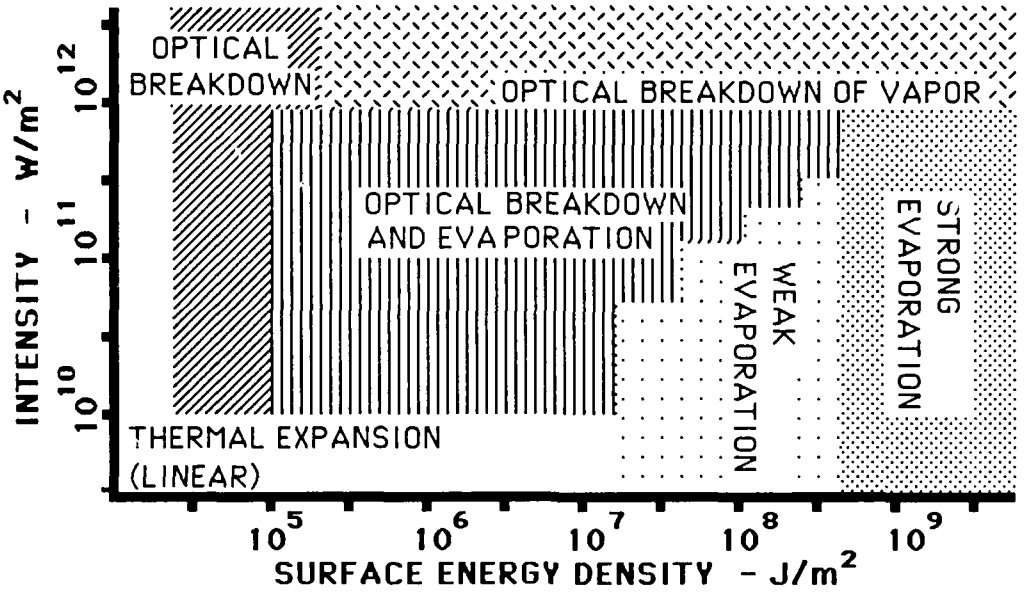

FIGURE 2

THE ANATOMY OF OPTOACOUSTIC SOUND GENERATION IN WATER WITH A 1.06 μm LASER

AS-86-475

normally about[3] $15\ m^{-1}$, which gives a surface energy density threshold of approximately $2 \times 10^7\ J/m^2$.

Above certain intensity and energy density thresholds, optical breakdown causes the physical properties of the medium to change. The intensity threshold for breakdown of water is strongly dependent on impurities such as suspended particles. The breakdown causes the water to become opaque. This is equivalent to a sudden increase in the absorption coefficient[4] and a consequent reduction in the evaporation threshold.

For 10.6 μm laser radiation on water, optical breakdown of the ejected vapor has been observed[5] above a threshold of $2 \times 10^{12}\ W/m^2$. Of course, there must also be sufficient energy density to produce the vapor in the first place. Therefore there is an energy density threshold as well.

Sound generation is by a combination of two main physical processes, the expansion of the material within the liquid due to physical or chemical changes and the recoil pressure at the surface from the ejected vapor. There have been a number of publications on this topic. A large proportion of the reported works have been for cases where most of the energy is spread over several megahertz.[6,7] The results reported by Hickman[8] were in the range of sonar frequencies but the experimental conditions were imprecise. The most extensive set of results were reported by Maccabee and Bell.[5,9,10,11] Their data covered a wide range of operating conditions. Their results showed significant finite amplitude distortion and extra attenuation of the acoustic pressure. Maccabee and Bell used a "rocket" model to predict the blast pressure and linear superposition to construct the acoustic pressure. They found that the model predictions were not consistent with the experimental results.[11] One likely contributor to the discrepancy is the nonlinear propagation of the acoustic output, because they used laser pulses of very high energy densities and intensities.

II. THEORY

The optoacoustic process being considered here is specifically that of dielectric breakdown, followed by a phase change from liquid to gas and the explosive expansion of the gas. The initial dielectric breakdown and phase change are not expected to significantly contribute to the sound generation process but they will consume a certain amount of energy. This may be considered as an overhead requirement. The explosive expansion is believed to be the main mechanism of sound generation. It will be modeled as a blast reaction. The blast model used is based on the work of A. N. Pirri[12,13] who successfully modeled the momentum transfer from a high powered laser blast to the surface of a solid. The model is general enough to be adapted to give a first approximation of the acoustic signals produced by a laser induced blast at the water surface. Our model is based on the more complicated of the two Pirri models. It is a two-stage model. It has a one dimensional stage where the blast front is assumed to rise vertically from the surface. This stage is essentially the "rocket model" used by Maccabee and Bell.[11] The second stage is a two-dimensional spreading regime where the blast expands outward over the surface. The model is illustrated in Fig. 3. The sound is assumed to propagate linearly and the underwater acoustic pressure signal is constructed from elementary constituents by linear superposition. In a theoretical study without experimental verification, Wu[14] followed this approach and obtained an estimate for the acoustic pressure. The deformation of the water surface is assumed to be negligible. The linear propagation and negligible deformation assumptions are some of the main shortcomings of this model. Nevertheless, under operating conditions where these assumptions are approximately valid, the model is expected to produce useful results. With further theoretical analysis supported by experimental measurements, more realistic models will evolve.

A. Basic Blast Theory

The nonlinear optoacoustic reaction is modeled as an explosive blast generated by the laser radiation at the water surface. The blast is assumed to be gas driven. For simplicity, let us assume that the gas within the blast is homogeneous. Given that the rate of energy input is sufficient to cause the blast wave to be supersonic, the relationship between the internal energy E_g, the pressure P_g, and volume V_g of the blast gas is given by the adiabatic gas equation,

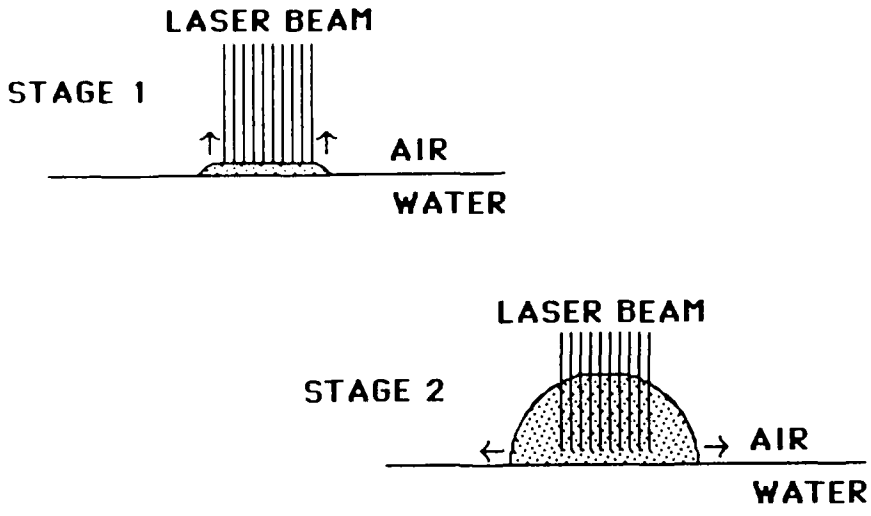

FIGURE 3
PIRRI'S SECOND BLAST MODEL

AS-86-476

$$P_g V_g = (\gamma - 1) E_g \quad , \tag{1}$$

where γ is the ratio of specific heats of the blast gas.

The movement of the blast front is governed by conservation of momentum considerations. The difference P_{DW} between the blast pressure P_g and the ambient pressure P_o must be equal to the rate of change of momentum per unit area at the blast front; therefore,

$$P_{DW} = P_g - P_o = (du/dt)^2 \rho_o/(\gamma + 1) \quad , \tag{2}$$

where ρ_o is the density of the surrounding fluid and u is the distance along the outward normal at the boundary of the blast.

Assuming isentropic flow, the coupling coefficient C_c between the blast pressure P_g and the pressure P_s at the water surface, quoting from Ref. 13, is given by the relationship,

$$C_c = P_s/P_{DW} = [(\gamma + 1)/2\gamma]^{2\gamma/(\gamma - 1)} \quad . \tag{3}$$

These three relationships form the basis of the blast theory used by Pirri to estimate momentum transfer from a high powered laser pulse to a solid surface.[13] Pirri's model has been modified to predict the acoustic waveform produced by a high powered laser pulse incident on a water surface.

B. Construction of the Acoustic Signal

The acoustic signal produced by a high powered laser beam striking the surface of the water will be constructed by superposition. The laser beam is assumed to have a uniform, circular cross section. For simplicity, the acoustic signal is observed at a distance that is sufficiently large to be outside the nearfield of the source to allow the use of farfield approximations.

The blast model program was implemented as a modular FORTRAN program that analyzes the received signal in three stages. First, the blast pressure and area of the

blast produced by the laser are computed as functions of time. Second, the program computes the time derivative of the downward pressure at the surface due to the blast using the blast pressure and area histories. Third, the acoustic signal at a given distance and angle is computed from the pressure derivative using Green's function and linear superposition. Spreading and absorption losses are taken into account. Movement of the water surface is neglected. Pirri initially used a spherical blast model,[12] but he later replaced it with a two-stage model,[13] shown in Fig. 3. The current model developed in this report is based on the latter. The laser pulse is assumed to be of constant power and beamwidth with a finite duration τ_p. The blast model was divided into two stages as shown in Fig. 3. In the first stage, the blast is a thin layer of vapor spreading upwards from the surface. Since initially the thickness is small compared to the width of the blast area, the expansion is mostly upwards and one dimensional, with negligible edge effects. In the one-dimensional stage the velocity of the blast front velocity du/dt is denoted by V_{DW}. Applying Eqs. (1) and (2) for the one-dimensional case and assuming that the laser intensity and beamwidth are constants, it can be shown that V_{DW} is also a constant. The expression for V_{DW}, originally derived by Raizer,[15] is

$$V_{DW} = [2(\gamma^2 - 1)\, I_o / \rho_o]^{1/3} \qquad (4)$$

where I_o is the laser intensity in W/m^2. Substituting for du/dt in Eq. (2) by the expression for V_{DW} from Eq. (4), the excess pressure within the blast volume is given by

$$p_{DW} = \rho_o V_{DW}^2 / (\gamma + 1) \qquad (5)$$

Applying the coupling relationship given in Eq. (3), the pressure p_{s1D} at the water surface in the one-dimensional stage is given by

$$p_{s1D} = p_{DW}\, C_c \qquad (6)$$

If the laser power is turned off while the blast is still one-dimensional, the pressure will decay as a planar blast[16] where the pressure $p_s(t)$ is given by

$$p_s(t) = p_{s1D}\, (t/\tau_p)^{-2/3} \quad ; \quad \text{for } (\tau_p \le t \le \tau_{2D}) \qquad (7)$$

where τ_p is the duration of the laser pulse and τ_{2D} is the duration of the one-dimensional stage. When the blast layer thickness approaches the width of the blast area, edge effects are no longer negligible and the pressure to expand outwards can no longer be ignored. At this point, the blast enters its second stage. The second stage is a two-dimensional spreading regime where the blast expands outward over the surface. The blast geometry is assumed to change from one-dimensional to two-dimensional when the height of the one-dimensional blast equals its diameter. This transition occurs at time τ_{2D}, given by[13]

$$\tau_{2D} = \int_0^{D_s} (1/V)\, dr \quad , \tag{8}$$

where D_s is the diameter of the one-dimensional blast area, also equal to the diameter of the laser illuminated area on the water surface, r is the displacement normal to the wavefront, and V is the velocity of the blast wave identically equal to du/dt in Eq. (2). If $\tau_p \geq \tau_{2D}$, then the velocity V of the blast front is equal to the constant V_{DW} and τ_{2D} is given by

$$\tau_{2D} = D_s/V_{DW} \quad , \tag{9}$$

If $\tau_p < \tau_{2D}$ then the velocity V of the blast front, after the cessation of the laser power input, is given by the planar decaying blast theory.[16] Quoting from Ref. 13, τ_{2D} is then given by

$$\tau_{2D} = [2/(3\, V_{DW}^{3/2}\, \tau_p^{1/2})]\, [D_s^{3/2} - (V_{DW}\, \tau_p)^{3/2}] + \tau_p \quad ; \quad \text{for } (\tau_p \leq t \leq \tau_{2D}) \ . \tag{10}$$

After time τ_{2D} the blast is assumed[13] to decay according to cylindrical blast theory irrespective of any additional laser input energy. The equation for the pressure is given by

$$p_s = p_{s1D}\, (\tau_{2p} / \tau_{2D})^{2/3}\, (\tau_{2D} / t) \quad , \tag{11}$$

where $\tau_{2p}=\tau_p$, if $\tau_p<\tau_{2D}$ or $\tau_{2p}=\tau_{2D}$, if $\tau_p \geq \tau_{2D}$. An illustration of the surface pressure as a function of time is given in Fig. 4.

Using the expression for a pressure source, the acoustic pressure p_L at a point (x_o, y_o, z_o) in Cartesian coordinates in a lossless medium is given by

$$p_L = \iint (\partial p_s(t-R/c)/\partial t) / (2\pi cR)\, dy\, dx \quad . \tag{12}$$

It is assumed that the blast is cylindrically symmetric with a radius r which varies with time t. R is the distance from the point (x, y, 0) on the surface to the hydrophone at (x_o, y_o, z_o). For simplicity, and without loss of generality, let the blast area be centered about the origin and $y_o = 0$. Therefore, R is given by

$$R = \sqrt{((x - x_o)^2 + y^2 + (z - z_o)^2)} \quad . \tag{13}$$

Then, the distance R_o from the center of the blast area to the hydrophone is simply

$$\sqrt{x^2_o + z^2_o} \quad .$$

When the hydrophone is in the farfield, R may be approximated by

$$R \approx \sqrt{((x - x_o)^2 + (z - z_o)^2)} \quad , \tag{14}$$

which is independent of y. Assuming that the blast gases are well mixed, the surface pressure and its rate of change will be uniform within the blast area. Assuming also that the pressure at the boundary of the blast area decays to zero over a finite transition region or skirt of width h, the expansion of the integral with respect to y for any time t may be expressed as

$$\int_{-\infty}^{\infty} (\partial p_s/\partial t)\, dy = \int_{-(y_1-(hr/2y_1))}^{(y_1-(hr/2y_1))} (\partial p_s/\partial t)\, dy + 2(hr/y_1)(p_s/r)V_s$$

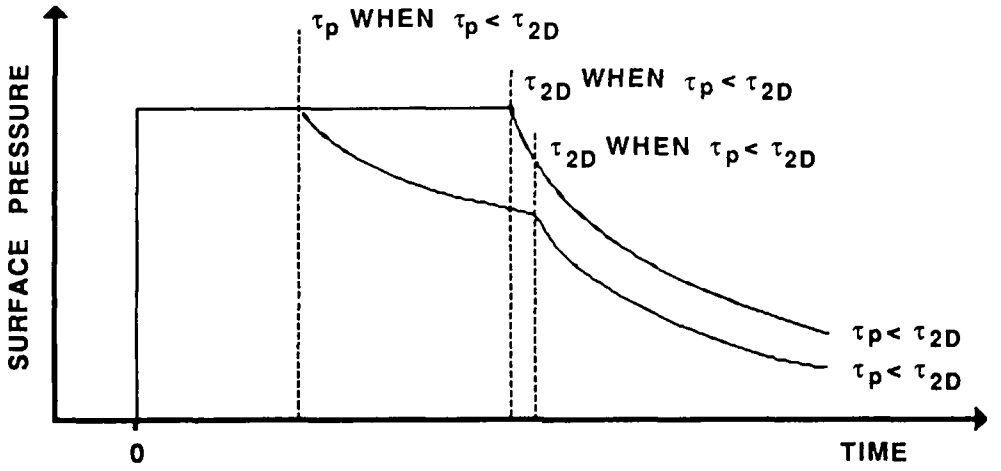

FIGURE 4
PRESSURE HISTORY AT THE WATER SURFACE

ARL:UT
AS-86-477
NPC - GA
1 - 9 - 86

$$+ 2 \int_{(y_1-(hr/2y_1))}^{(y_1+(hr/2y_1))} (\partial p_S/\partial t)\,((y-(y_1-(hr/2y_1))/(hr/y_1))\,dy \quad , \tag{15}$$

where V_S is the surface velocity of the blast boundary, and the limit y_1 is a function of the value of x and the radius r of the blast area,

$$y_1 = \sqrt{(r^2 - x^2)} \quad . \tag{16}$$

Figure 5 shows a model of the surface pressure distribution. The first term in Eq. (16) is due to the rate of change of blast pressure within the homogeneous blast area, the second term is the contribution from the rate of change of pressure at a point within the skirt due to the movement of the blast boundary, and the last term is due to the pressure change in the skirt of the blast. Equation (15) simplifies to

$$\int_{-\infty}^{\infty} (\partial p_S/\partial t)\,dy = (\partial p_S/\partial t)\,y_1 + rp_S V_S/y_1 \quad , \tag{17}$$

which is independent of h, the width of the skirt of the blast area. The acoustic signal at a given distance and angle is computed from the downward surface pressure by taking into account the spreading. Since the time delay term R/c is a function of x, the radius r of the blast is also dependent on x and the relationship between $(\partial p_S(t-R/c)/\partial t)$ and x becomes rather complicated particularly when the blast velocity is supersonic; therefore, the remaining integral with respect to x is carried out numerically. The blast surface pressure, its time derivative, and the blast radius as functions of time are generated as spline curves to ensure continuity of the first derivative.

After the acoustic signal for a lossless medium has been constructed, the absorption losses are calculated using the frequency dependent absorption coefficient α in dB/m from Schulkin and Marsh,[17]

$$\alpha = (ASf_T f^2)/(f_T^2 + f^2) + Bf^2/f_T \quad , \tag{18}$$

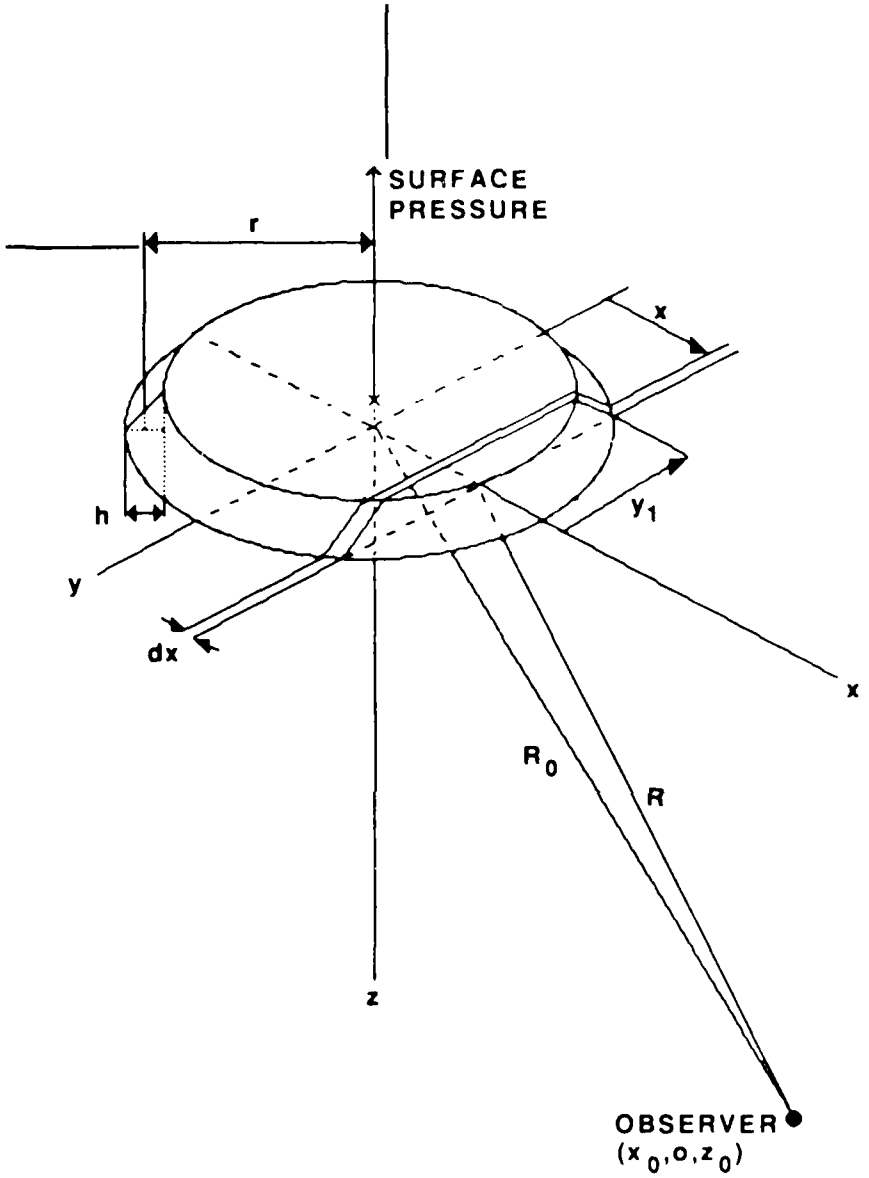

FIGURE 5
MODEL OF THE SURFACE PRESSURE DISTRIBUTION

ARL UT
AS-86-478
NPC-GA
1-9-87

where

f = frequency in kHz,

$f_T = 21.9 \times 10^{(6-1.52/(T+273))}$, (19)

$A = 0.00002034$,

$B = 0.00002931$,

S = salinity in parts per thousand, and

T = temperature in degrees Celsius.

The absorption coefficient is then applied to the signal in the frequency domain after taking its Fourier transform. The final signal is then reconstructed from its transform.

C. Theoretical Results

An example of the theoretical estimate of the acoustic signal waveform and its energy density spectrum is shown in Figs. 6(a) and (b), respectively. Referring to the geometry in Fig. 5, the range from the source to the point of observation R_0 is 1.2 m and the ray path makes an angle with the downward vertical θ_0 of 45°. Since the blast very rapidly enters the second stage and expands outward supersonically, the contribution from the edge of the expanding and decaying second stage of the blast arrives before the main contribution from the more impulsive first stage, thus giving the acoustic pulse a gradual buildup in pressure before the arrival of the main pressure pulse. The main pressure pulse is very short, and is followed by a rarefaction phase to complete the cycle. The energy density spectrum plot shows the energy mainly concentrated below 200 kHz. Below 50 kHz the spectrum falls off due to the transfer function of the optoacoustic process, which decreases with decreasing frequency. Above 100 kHz the spectrum abruptly falls off due to diffraction and, to a lesser extent, absorption losses. The absorption loss increases with frequency and range. The diffraction effect becomes significant when the resolved physical size of the optoacoustic source in the direction of the ray path from the source to the point of observation exceeds the acoustic wavelength. The model assumes that the optoacoustic source is infinitely thin. Therefore, any diffraction effects must come from the resolved dimensions of the blast area in the direction of the ray path; the resolved length of the source in this direction is approximately the diameter of the blast

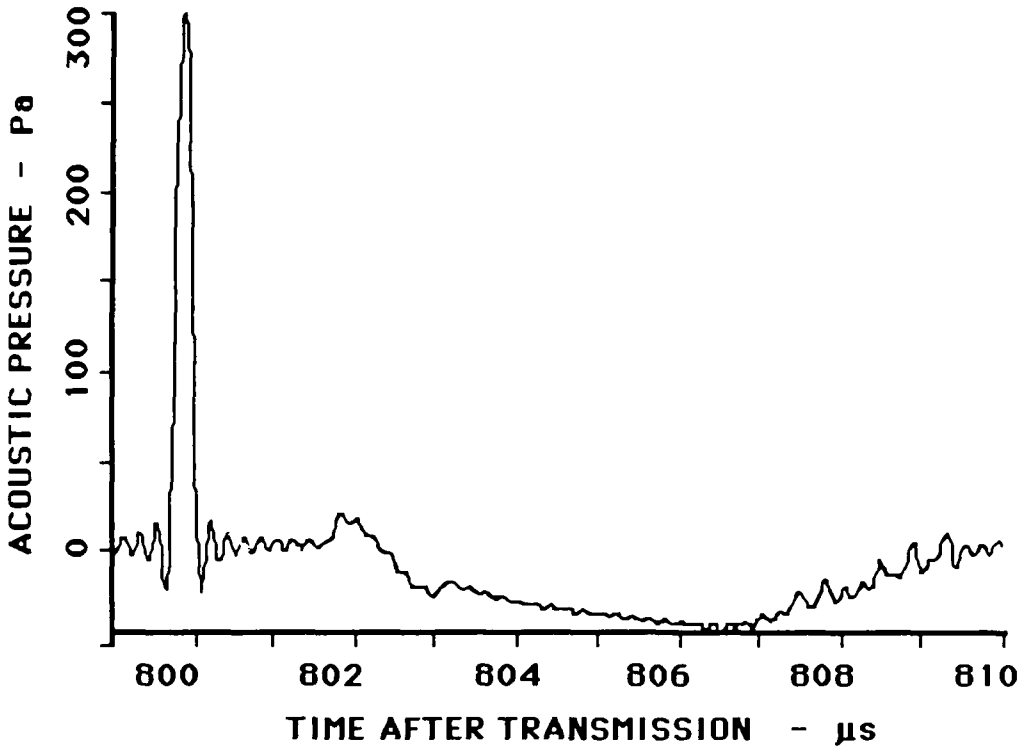

FIGURE 6 (a)

AN EXAMPLE OF THE THEORETICALLY PREDICTED WAVEFORM FOR THE FOLLOWING CONDITIONS:

$R_0 = 1.2$ m

$\theta_0 = 45°$

laser pulse energy = 0.13 J

laser beam area = 8 mm^2

laser pulse duration = 3.5 μs

ratio of specific heats of blast gas = 1.2

AS-86-479

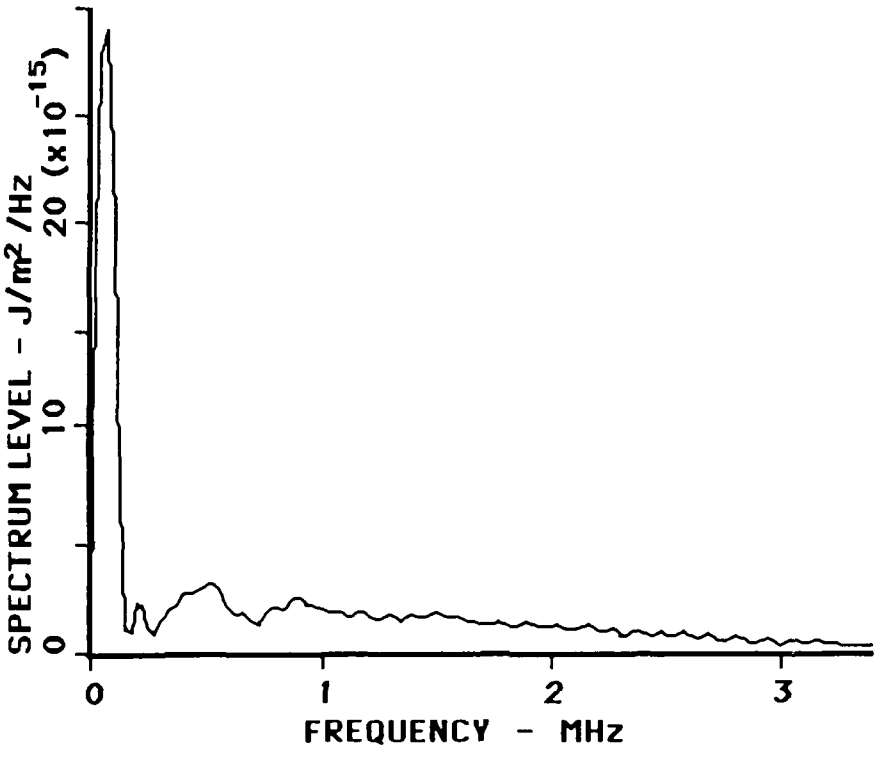

FIGURE 6(b)

THE ACOUSTIC ENERGY DENSITY SPECTRUM OF THE PRESSURE WAVEFORM IN FIG. 6(a)

AS-86-480

area multiplied by sin (θ_o), where θ_o is the angle between the downward vertical and the hydrophone. This explanation was found to be consistent with the observed upper cutoff frequency.

D. Comparison of Theoretical Predictions with the Results of Maccabee and Bell

Maccabee and Bell[11] presented a number of experimental results of peak acoustic pressure as a function of laser pulse energy at the 109th Meeting of the Acoustical Society of America. One set of their data satisfies the farfield criterion for which the present model is applicable. The comparison between the peak pressures predicted by our model and their experimental data is shown in Fig. 7. It can be seen that there is some agreement between them, although the theoretical and experimental waveforms, which are not shown here, were quite different. The difference in the waveforms was expected because our model assumes only linear propagation while the experimental data appeared to be shock limited. Nevertheless, within the band of the signal frequencies and over such a short distance, the extra attenuation due to nonlinear propagation was not expected to be very significant and therefore the comparison of the peak pressure of the leading edge of the pulse is expected to be valid. The results show that at the lower energy levels, the theory appears to over-estimate the peak pressures. The way the theory and experimental results diverge suggest that a certain amount of the laser pulse energy may not be directly contributing to the blast. This is not inconsistent with the current understanding of nonlinear optoacoustic processes in which the medium has to undergo a local change of state, such as a dielectric breakdown, before the blast can take place. The change of state will consume a finite amount of the laser energy leaving the remainder to fuel the optoacoustic generation process which is modeled as a blast. Therefore, a constant laser energy density overhead should be expected. From Fig. 7, it is estimated that the energy density overhead is about 3.3×10^3 J/m^2.

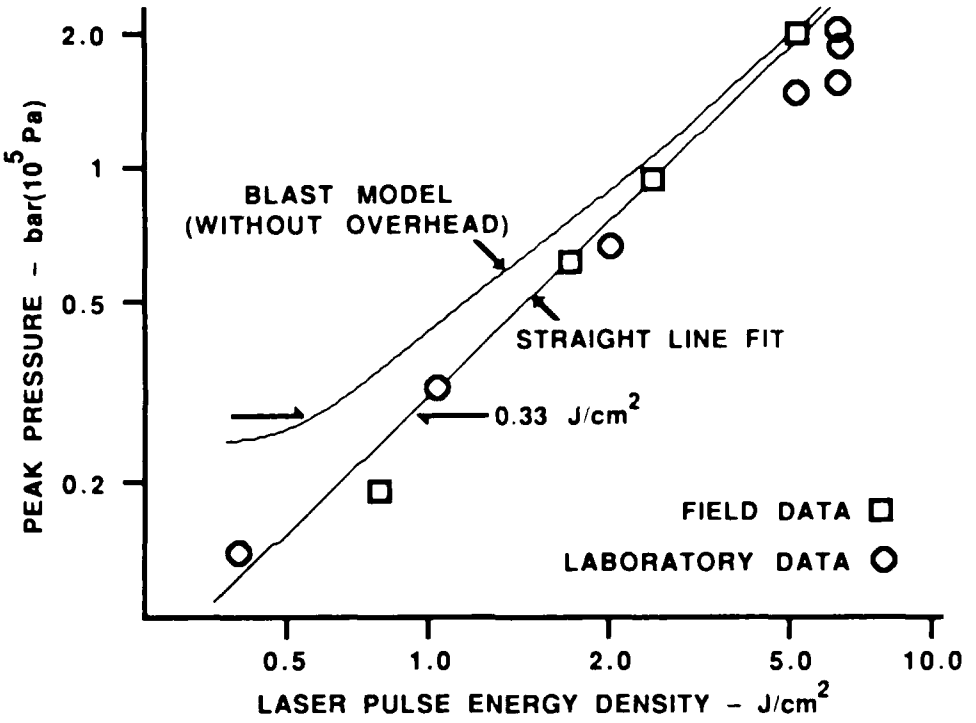

FIGURE 7
COMPARISON OF THEORETICAL MODEL PREDICTIONS OF PEAK PRESSURE WITH THE EXPERIMENTAL DATA FROM MACCABEE AND BELL

THE EXPERIMENTAL CONDITIONS WERE:

$R_0 = 0.5$ m
$\theta_0 = 0°$
LASERBEAM AREA = 0.2 cm^2
LASER WAVELENGTH = 1.06 μm

ARL UT
AS-86-481
NPC - GA
1 - 9 - 87

III. EXPERIMENT

Experiments were carried out to verify the blast model and to obtain a better understanding of the process. Due to the small amount of time and resources available at this stage of the contract, these investigations should be considered as preliminary. In these experiments, the specific goals are (1) to measure the energy density overhead, (2) to compare the predictions of the blast model with the practical results, and (3) to identify weaknesses in the blast model which need to be improved. From these results, recommendations for future work will be made.

A. Apparatus

The experimental arrangement is shown in Fig. 8. The laser used is an Apollo Nd:glass laser Model 22/A with a peak energy of 22 J and a wavelength of 1.06 μm. It is capable of producing an unmodulated pulse of up to 1 ms and a spot size of approximately 8 mm^2. A short laser pulse is achieved by putting a Pockels cell and polarizer in the laser cavity and using a Q-switch driver to modulate the Pockels cell. Each pulse lasted less than 3.5 μs and a train of up to five pulses at a maximum repetition rate of 10,000 pulses per second could be delivered. The control circuit determined the number of pulses and the timing between pulses. A fast photodetector connected to a Nicolet digital oscilloscope monitored the laser pulse. The laser beam was directed vertically down to the water surface by a prism and focused on the surface by a pair of lenses. The acoustic signal was detected by a hydrophone. The hydrophones used were the E8-59, E8-62, and H23. Detailed descriptions of the hydrophones are given in Appendix A. The outputs of the hydrophones were amplified and filtered through a 30 dB balanced amplifier or an HP465A 20 dB amplifier and followed by a KH3100 bandpass filter. The data were recorded on a Nicolet 4096 digital oscilloscope.

B. Noise and Multipath Suppression

In our experiments, we encountered numerous noise interference problems. The most persistent of these was the electrical noise pulse from the Q-switch driver. This noise pulse affected the performance of the control circuit and appeared in the output signals of the photodetector and the amplifiers. The Q-switch driver sent a sharp

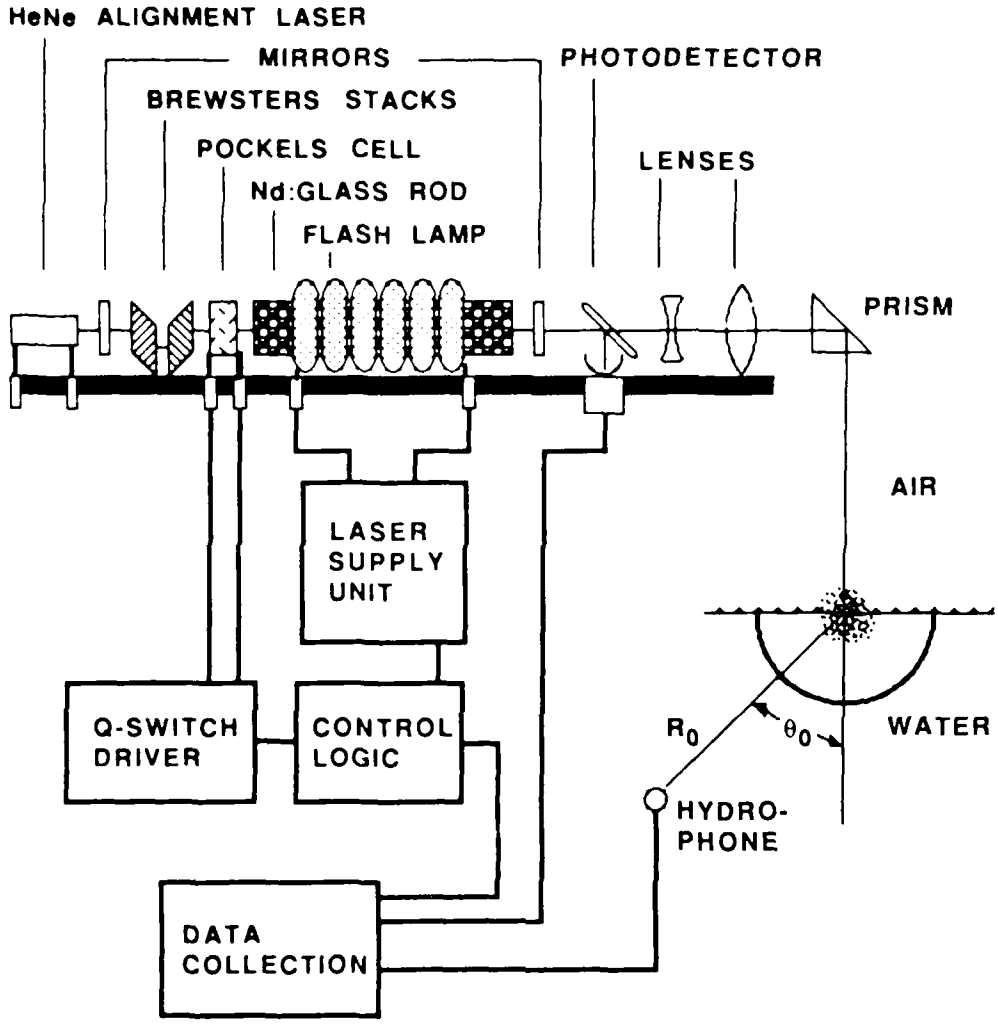

FIGURE 8
THE LABORATORY EXPERIMENT

ARL:UT
AS-86-482
NPC - GA
1 - 9 - 87

negative voltage spike through the power supply of the control circuit which occasionally caused the circuit to go into the hardware equivalent of an infinite loop. This problem was solved by putting a power diode in series with the power supply. We eliminated the noise in the photo-detector by building two spatially symmetric, voltage balanced photodetector circuits. One was open to the laser light and the other was covered. The difference of the two signals was the detected optical pulse of the laser. A description of the circuit is given in Appendix B.

The acoustic signal was contaminated by both electrical and acoustic noise. Due to the time delay between the firing of the laser and the arrival of the acoustic signal, the direct electrical interference from the laser system could be gated out. However, residual ringing from the laser interference persisted long enough to contaminate the acoustic signal as a low frequency background. This was removed by digital filtering.

Acoustic and electrical noise from all other sources were random and they were reduced by taking ensemble averages. An ensemble average of ten was usually enough to yield a clean signal, with a signal-to-noise ratio (S/N) of about 40 dB.

Multipath interference problems were avoided by careful design of the layout. The first multipath to reach the hydrophone is the reverberation from the bar on which the hydrophone is mounted. By putting the hydrophone on a small extension, the multipath was sufficiently delayed so it could be gated out. The other source of reverberation was the walls of the tank. Fortunately our tank is large enough that these would arrive well after the signal.

C. Procedure

Before beginning the experiment, the laser power supply and Q-switch driver were switched on and allowed approximately 5 minutes to stabilize. Then, the pulse repetition sequence on the pulse controller was set to the required values. The hydrophone was put into position. While running the experiment, the laser coolant temperature, the photodetector's output, and the received acoustic signal were monitored. The E8 hydrophones were calibrated from 100 kHz to 1 MHz, and in this band their response is known to be flat. Their outputs were bandpass filtered from 75 kHz to 500 kHz to avoid aliasing because the data recording system could

only sample at 2 MHz. The H23 hydrophone was calibrated from 1 kHz to 150 kHz and within this band its response was approximately flat; its output was bandpass filtered over the same band.

D. Experimental Results

The acoustic signal energy density was measured at a hydrophone located approximately 1.2 m directly below the source (R_0 = 1.2 m and θ_0 = 0 in Fig. 8). The measured acoustic energy density is plotted as a function of corresponding laser pulse surface energy density in Fig. 9. The data were from a set of multiple pulse firings of the laser. In each firing, a sequence of five pulses was delivered to the water surface. The pulse repetition period was 0.125 ms. At laser energy levels below 4 J/cm^2, it appears that the data lie approximately on a straight line irrespective of the position of the pulse in the sequence, except for the lowest data point where, referring to Fig. 2, the laser energy density may be too low for a blast to fully develop. At higher energy density levels, it appears that there are some anomalies and that the position of the pulse in the sequence has some influence on the result. The second and subsequent pulses appear to have a slightly higher energy conversion efficiency than the first pulse. It is speculated that the after-effects of the first pulse caused the energy density overhead requirement for the subsequent pulses to be reduced. Fitting a straight line through the data from the first pulses of each sequence, the optical energy density overhead requirement for a single laser pulse was found to be 16×10^3 J/m^2. This result does not agree with the corresponding result from the data of Maccabee and Bell. A possible cause of the discrepancy is the difference in the laser wavelengths. Maccabee and Bell used a laser of wavelength 10.6 μm while we used 1.06 μm. At the latter wavelength, the laser absorption coefficient in water is significantly lower, and therefore it is logical to expect that more energy will be dissipated into the interior of the water before the start of a nonlinear reaction at the surface.

The peak acoustic pressure was plotted against the peak laser power to determine the empirical relationship between them. The results are shown in Fig. 10. Unlike the energy density comparison, it appears that, at laser peak intensities greater than 100 kW/m^2, the second and subsequent pulses have lower peak acoustic pressures for the same peak laser intensity. The data point at the lowest peak acoustic pressure and laser intensity appears to be anomalous. As with the lowest data point in

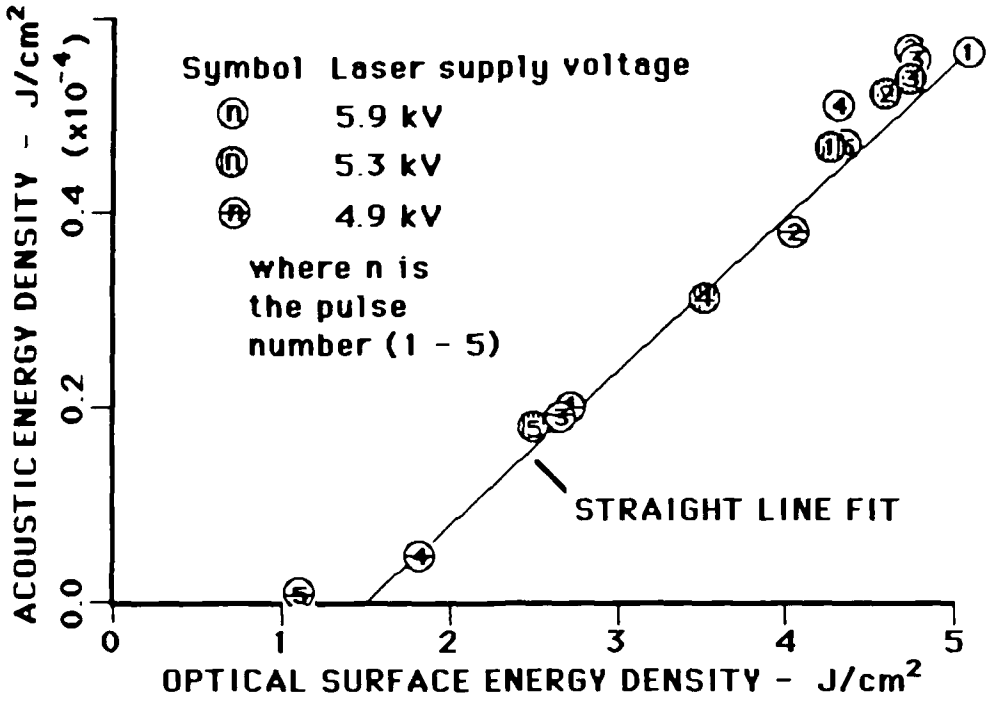

FIGURE 9

EXPERIMENTAL MEASUREMENTS OF ACOUSTIC ENERGY DENSITY AS A FUNCTION OF OPTICAL ENERGY DENSITY THREE PULSE TRAINS OF FIVE PULSES EACH. A straight line fit is shown through the first pulses. The experimental conditions were:

$R_0 = 1.2\,m$

$q_0 = 0°$

laser beam area = $8\,mm^2$

laser pulse duration = $3.5\,\mu s$

receiver bandwidth extended from 75 kHz to 500 kHz

AS-86-483

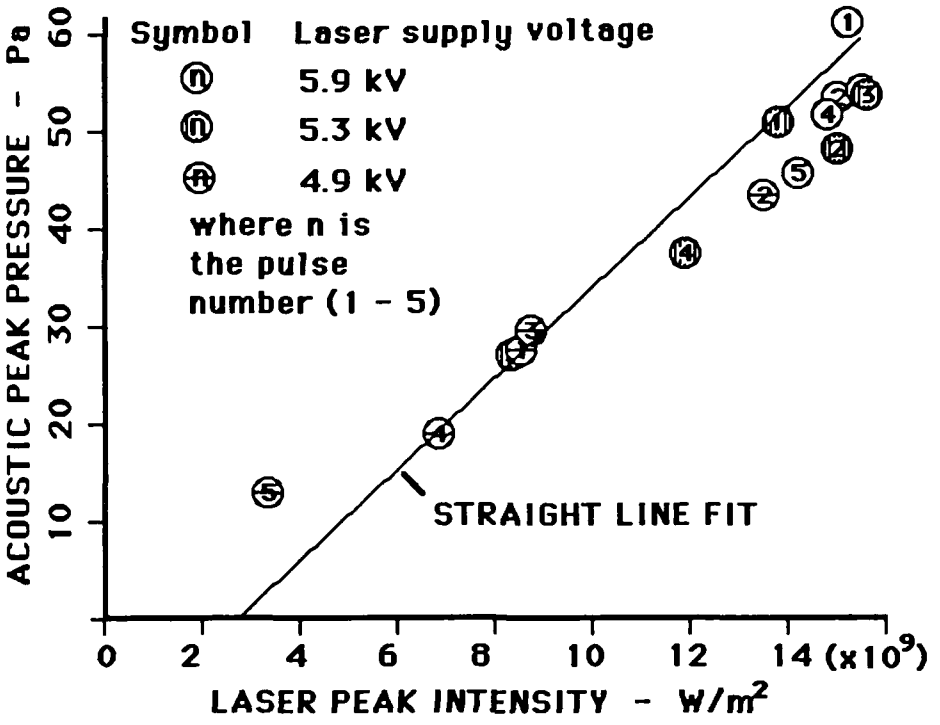

FIGURE 10

EXPERIMENTAL MEASUREMENTS OF PEAK ACOUSTIC PRESSURE AS A FUNCTION OF PEAK OPTICAL INTENSITY, FROM THREE PULSE TRAINS OF FIVE PULSES EACH. A straight line fit is shown through the first pulses. The experimental conditions were:

$R_0 = 1.2$ m

$\theta_0 = 0°$

laser beam area = 8 mm^2

laser pulse duration = 3.5 μs

receiver bandwidth extended from 75 kHz to 500 kHz

AS-86-484

Fig. 9, it is speculated that, referring to Fig. 2, the laser intensity may be too low for a blast to be properly triggered. Fitting a straight line through the first pulse data points, the results indicate that a peak laser intensity of approximately $3 \times 10^9 W/m^2$ is the minimum peak intensity for a blast to be properly triggered.

In Fig. 11, the acoustic pulses from single laser pulses of different energy levels are compared. The results in Fig. 11 were obtained using the E8-59 hydrophone, covering the frequency band from 100 kHz to 500 kHz. In Figs. 12(a) and (b), the energy density spectra of the pulses are compared. The spectra in Fig. 12(a) were generated directly from the pulses shown in Fig. 11. Those of Fig. 12(b) were from pulses of similar energy detected by the H23 hydrophone covering the frequency range from 1 kHz to 150 kHz. The spectra at the two energy levels were found to be of the same shape. A doubling of the laser pulse energy produced an increase of approximately 6 dB in the acoustic energy density spectrum.

The acoustic signals at angle $\theta_0 = 0$ and 45° were also measured. Examples of their energy density spectra are compared in Fig. 13. The spectrum from the $\theta_0 = 45°$ case appears to cut off at approximately 175 kHz, while that of the $\theta_0 = 0°$ case cuts off at approximately 450 kHz.

The cutoff in the 45° case is due to the frequency dependence of the source directivity function. At wavelengths approaching the resolved width of the blast in the hydrophone direction, the contributions from different parts of the blast area will combine destructively. The width of the blast can be estimated from the -3 dB cutoff frequency and the pressure distribution across the blast aperture. The pressure distribution across the blast area could probably have been deduced from a more detailed set of acoustic measurements but at this stage, for simplicity, a simple distribution function was assumed. The derivation of the equations is presented in Appendix C. Assuming an even distribution of the surface pressure gives a width of 1.08 mm, which is an area of 0.92 mm^2. Assuming a Gaussian distribution gives a width of 0.72 mm, which is an area of 0.41 mm^2. The area we determined using laser burns on photographic paper is 8 mm^2. If this model is valid, then the acoustic results would suggest that the laser energy is mainly concentrated in a much smaller area than the burn mark would indicate. Although the burn method of determining the blast area is somewhat inaccurate since it does not linearly represent the spatial distribution

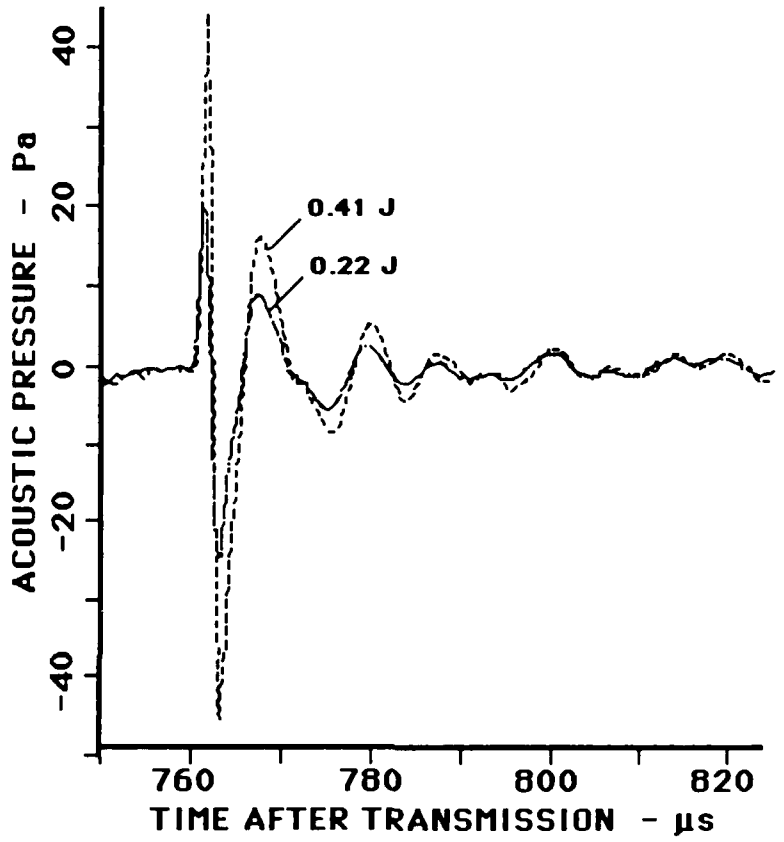

FIGURE 11

AN EXAMPLE OF THE EXPERIMENTALLY MEASURED ACOUSTIC WAVEFORMS USING THE E8-59 HYDROPHONE AT:

$R_0 = 1.2$ m

$\theta_0 = 0°$

laser pulse energy = 0.22 J and 0.41 J

laser supply voltage = 4.9 kV and 5.9 kV, respectively

laser beam area = 8 mm^2

laser pulse duration = 3.5 μs

AS-86-485

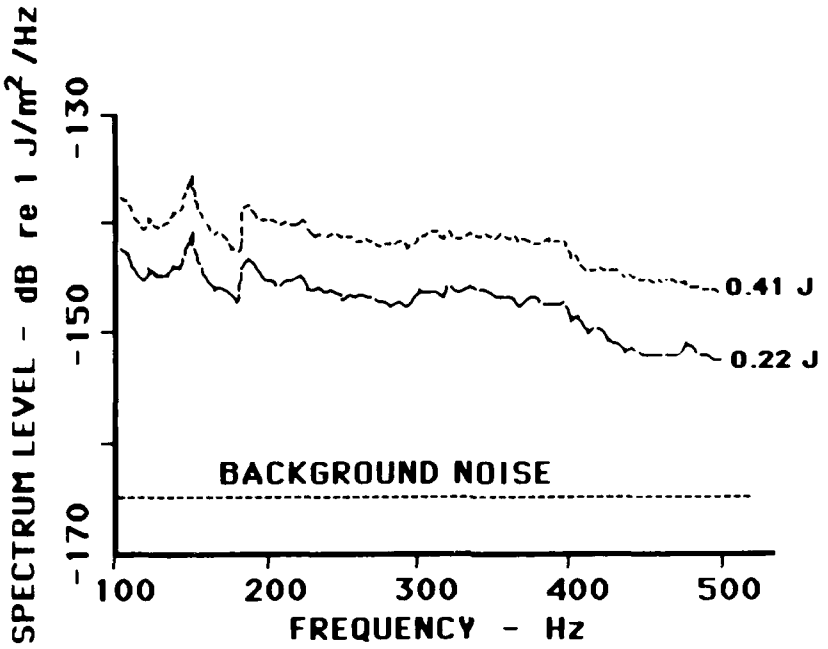

FIGURE 12 (a)

THE ENERGY DENSITY SPECTRA OF THE ACOUSTIC PULSES IN FIG. 11

AS-86-486

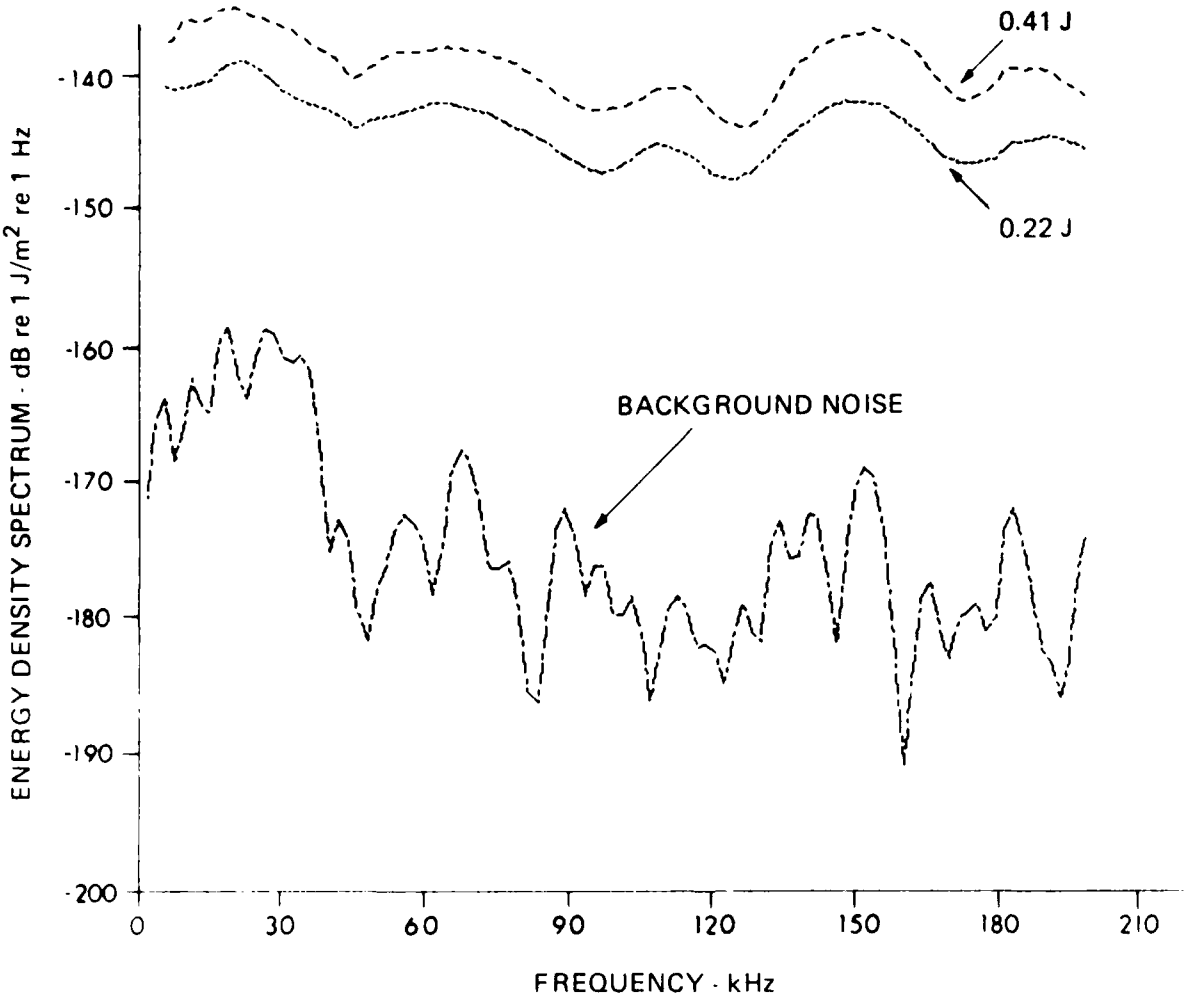

FIGURE 12 (b)
THE ENERGY DENSITY SPECTRA OF ACOUSTIC PULSES DETECTED BY THE H23 HYDROPHONE OF THE SAME LASER ENERGY LEVELS AS IN FIG. 11

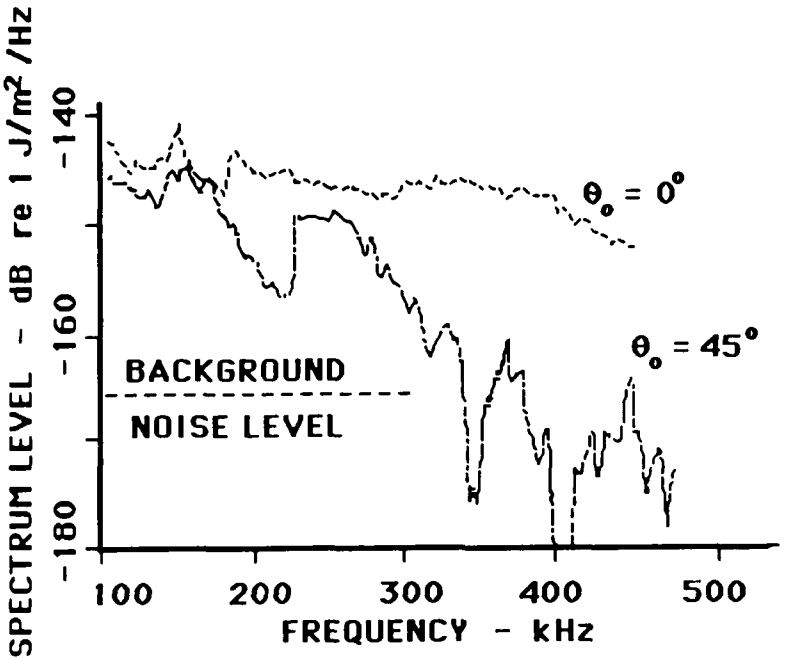

FIGURE 13

COMPARISON OF THE SPECTRA FROM THE $\theta_0 = 45$ AND THE $\theta_0 = 0°$ CASES

AS-86-487

of the laser energy, it is difficult to believe that it could be in error by an order of magnitude. A possible cause for the discrepancy may be the deformation of the water surface, which is ignored in the current model. In the published literature, small, approximately spherical depressions in the water surface have been reported.[6] The optoacoustic source distribution is expected to conform to the depression, which will have the effect of raising the diffraction limited upper cutoff frequency in the $\theta_0 \neq 0$ directions. The cutoff at 0° may be due to either the thickness of the layer of effective sound sources or the upper frequency cutoff of the laser pulse itself. Assuming the first of the two explanations, and assuming a vertical exponential distribution of the source density function, the 1/e depth of the optoacoustic source is estimated to be 0.084 mm. However, since the length of the laser pulse, at 3.5 μs, has a cutoff frequency of around 300 kHz, it is more likely that this is the cause of the upper frequency cutoff. Currently, we have no way of determining the thickness of the sound source layer but the above results show that it must be equal to or less than 0.084 mm.

E. Comparison of Experimental and Theoretical Results

Since the signal was bandpass filtered to retain only the frequency components within the calibrated frequency range of the hydrophones, it was necessary to band pass filter the theoretical signal over the same band before direct comparisons could be made. The E8 hydrophones were calibrated from 100 kHz to 1 MHz, and in this band their response is known to be flat. Their outputs were bandpass filtered from 75 kHz to 500 kHz to avoid aliasing because the data recording system could only sample at 2 MHz. The H23 hydrophone was calibrated from 1 kHz to 150 kHz and within this band its response was approximately flat; its output was bandpass filtered from 1 kHz to 150 kHz.

In Fig. 14, an example of the measured acoustic waveform is compared with the theoretical model prediction. The theoretical model includes a rectangular bandpass filter from 75 kHz to 500 kHz to approximately match the bandpass filtering of the experimental data. The prediction was based on a laser spot size of 8 mm^2, as measured by the burn method. The spot size inferred from the high cutoff of the spectrum was not used because it was only an indirect estimate based on certain assumptions. As indicated in Section II.D, a certain amount of laser energy overhead loss must be allowed for. There was no way to measure it, but it was found by trial and

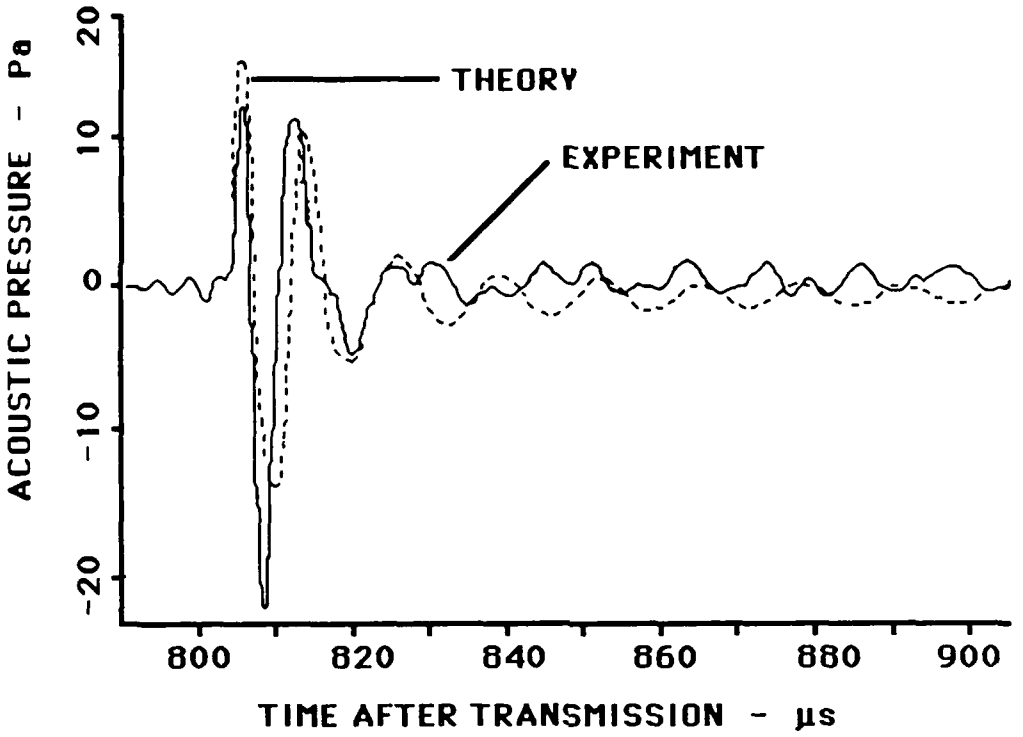

FIGURE 14 (a)

COMPARISON OF AN EXPERIMENTALLY MEASURED ACOUSTIC WAVEFORM WITH THE CORRESPONDING THEORETICAL MODEL PREDICTION. The experimental conditions were:

$R_0 = 1.2$ m

$\theta_0 = 45°$

laser pulse energy = 0.22 J

laser beam area = 8 mm^2

laser pulse duration = 3.5 μs

AS-86-488

error that a value of 0.13 J gave good agreement with experimental results. This figure is expected to be strongly dependent on the laser spot size. In Fig. 14(a), the waveforms are compared. There is much ringing and this is mainly due to the bandpass filter. The theoretical and experimental waveforms appear similar. However, since the expected acoustic signal is a short impulse, the similarity between the theoretical and experimental waveforms is mostly a product of the bandpass filtering rather than any fundamental agreement between theory and practice. Nevertheless, the comparison is encouraging since it shows that the model predicts a signal pressure level that is in approximate agreement with the experimental result. In Figs. 14(b) and (c), the corresponding energy density spectra are compared. The results show differences in the shapes of the spectra. These differences are most likely due to the oversimplicity of the model.

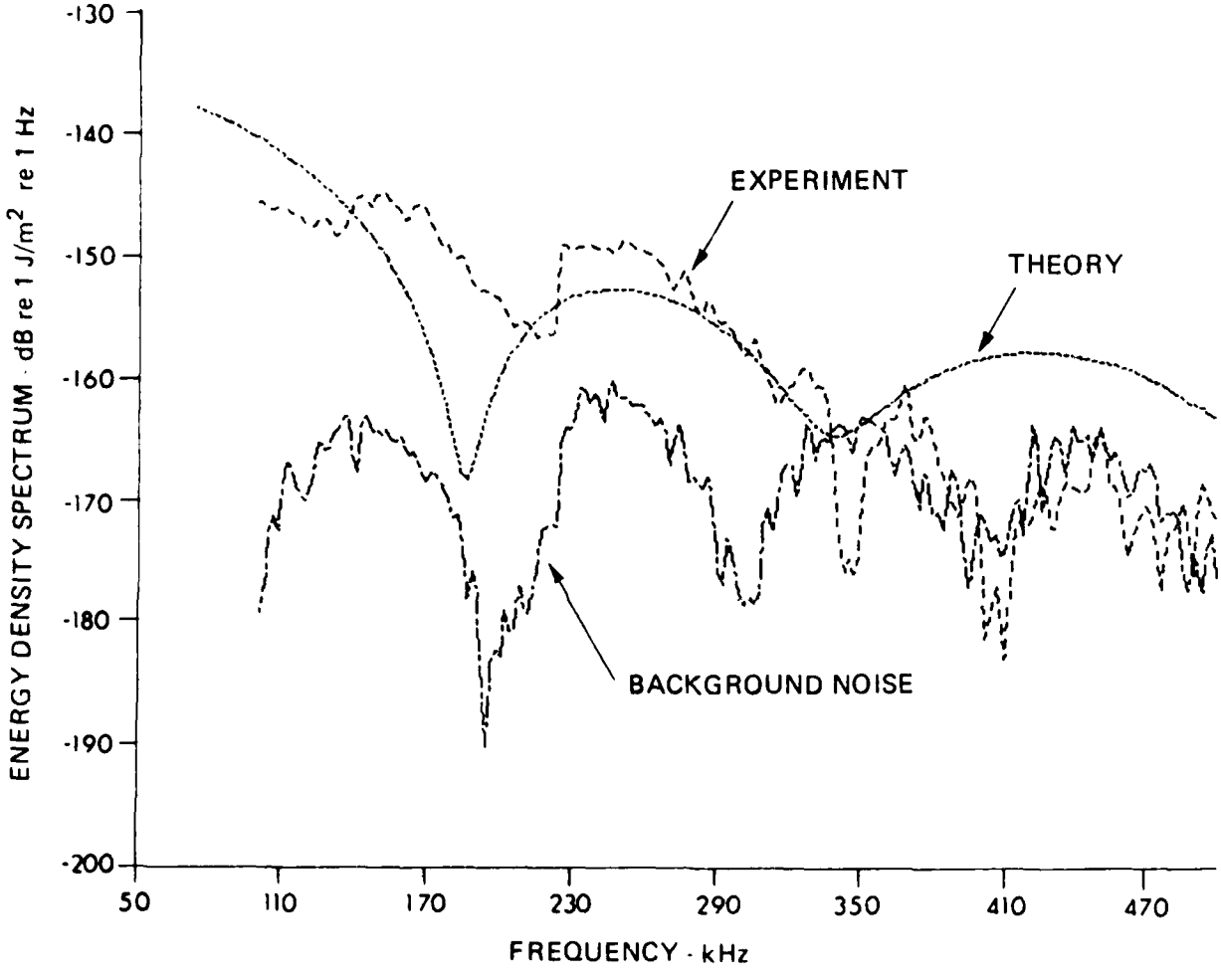

FIGURE 14 (b)
A COMPARISON OF THE ENERGY DENSITY SPECTRA OF THE THEORETICAL AND MEASURED WAVEFORMS IN THE 75 - 500 kHz BAND USING THE E8-59 HYDROPHONE

ARL UT
AS 86 115
NPC GA
3 28 86

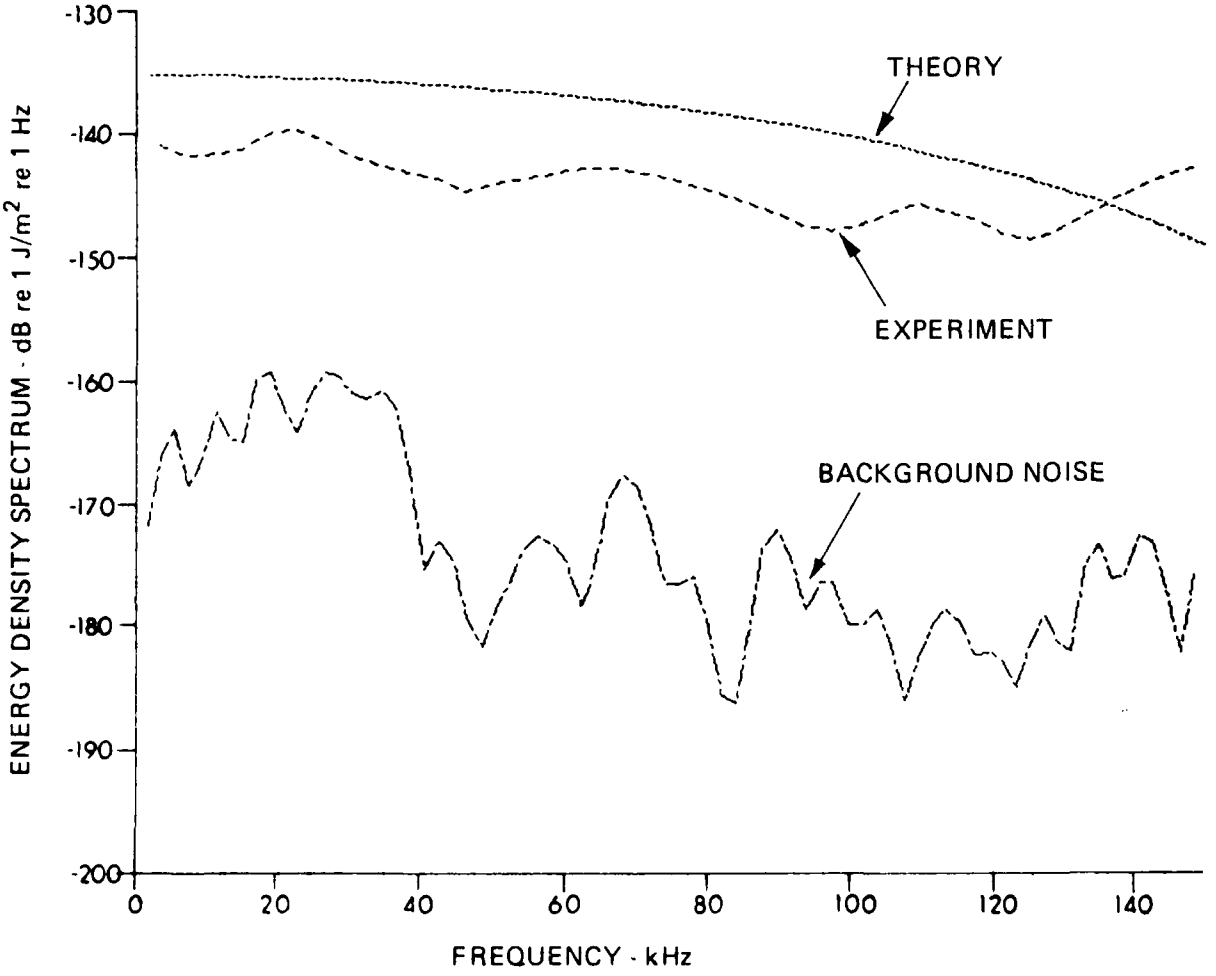

FIGURE 14 (c)
A COMPARISON OF THE ENERGY DENSITY SPECTRA OF THE THEORETICAL AND MEASURED WAVEFORMS IN THE 1 - 150 kHz BAND USING THE H23 HYDROPHONE

ARL:UT
AS - 86 - 116
NPC - GA
3 - 28 - 86

IV. CONCLUSIONS

A nonlinear process of optoacoustic sound generation was modeled. The process was one of inducing an explosive reaction at the water surface. The explosive reaction is induced by using a high intensity laser pulse. The experimental results suggest that the sequence of events might be as follows: the leading edge of the laser pulse causes a phase change, most probably a dielectric breakdown, within a thin surface layer. For a 1.06 μm laser wavelength, it was found that 16×10^3 J/m^2 was required to produce the phase change. As a result of the breakdown, the remaining laser energy is absorbed by the layer. Since the layer is very thin, the absorbed energy causes an explosive expansion.

A blast model for estimating the momentum transfer from a laser pulse to a solid surface[12,13] was adapted to give an approximate model of the optoacoustic sound generation process in water. Bearing in mind that this is only a first attempt, the model gave estimates of the acoustic output signal which were in reasonable agreement with our experimental results as well as some of those of Maccabee.[11] The signal levels predicted were approximately consistent with the measured data.

There were a number of discrepancies between theory and experiment. The shape of the signal spectrum as predicted by the theory did not match the measured spectrum. The most probable cause is the assumption in the model that the laser pulse is rectangular, while the actual laser pulse in the experiment was more rounded with a short rise time and a much longer fall time. The measured upper cutoff frequency in the off axis case was significantly higher than the corresponding model prediction. This is speculated to be due to the deformation of the water surface which is neglected in the current model.

In conclusion, a successful first attempt has been made to model a nonlinear optoacoustic sound generation process. This model should be further developed to give a more accurate representation of the process and thus provide a better understanding of its physics.

V. FUTURE PLANS

Improvements are planned in both the theoretical model and in the experimental apparatus.

The theoretical model needs to be improved in several respects. The experimental results indicated that a portion of the laser energy may have been used to produce a phase change within a thin layer of the water before a blast can be generated; this needs to be verified by a quantitative theoretical analysis. The experimental results obtained so far indicate that the shape of the laser pulse and the deformation of the water surface are important; therefore the model should be modified to take these into account. Consequently, a model for the deformation of the water surface is also required. Photographic data[6] suggest that there is a spherical indentation of the surface due to the formation of a gas bubble as shown in Fig. 15. Finally, to extend the validity of the model it is necessary to include nonlinear propagation effects using a numerical method such as that of Hall and Holt.[18] Their method uses finite element analysis in a dynamic frame of concentric elements, as illustrated in Fig. 16.

From our experience in the laboratory, a number of improvements in the experimental apparatus are required in order to provide a more complete set of data. An optical fiber system to detect laser light above and below the water line is required to monitor the history of the blast and verify the model of the blast process, as illustrated in Fig. 17. This will allow us to determine when the surface has reached a state of dielectric breakdown. It may also allow the scattering of the laser light by the blast to be studied. A better hydrophone, with a wider bandwidth from about 1 kHz to 10 MHz, is required. For this application, commercially available shock probes may be adequate. Finally, to keep up with the increased data rate, the data acquisition hardware needs to be upgraded to handle sampling rates of at least 10 MHz per channel.

The above improvements in the theoretical model and the experimental apparatus will enable us to investigate the nonlinear optoacoustic processes in greater depth. We will be able to observe the formation of the blast with acoustic and optical sensors. With the optical sensors, we will determine the proper sequence of events of

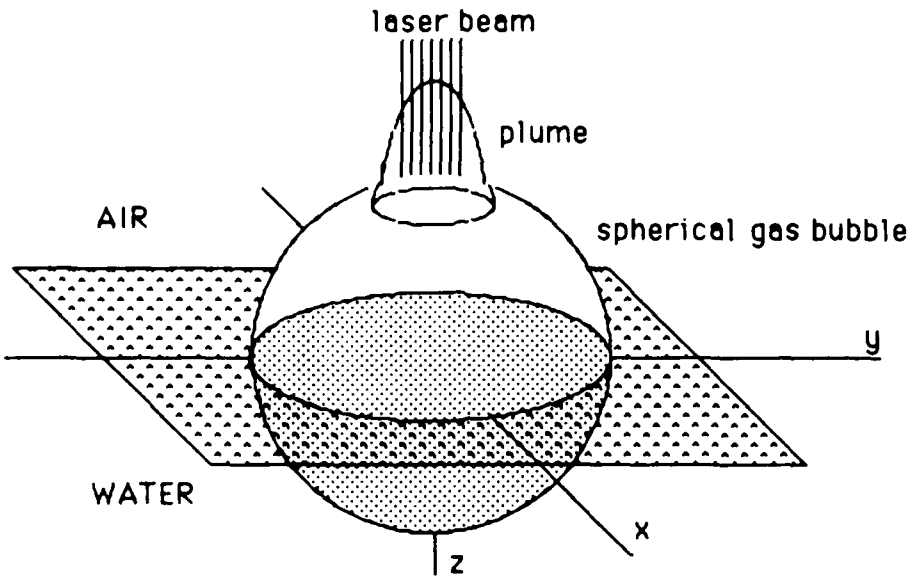

FIGURE 15

A POSSIBLE MODEL OF THE SURFACE DEFORMATION

AS-86-489

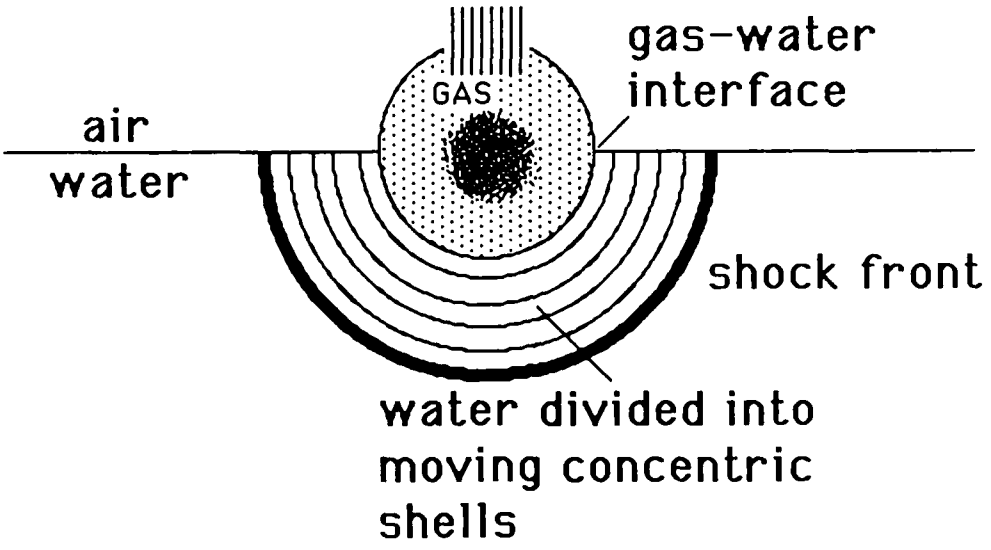

FIGURE 16

ANALYSIS OF NONLINEAR PROPAGATION IN THE SPHERICALLY SYMMETRIC CASE

AS-86-490

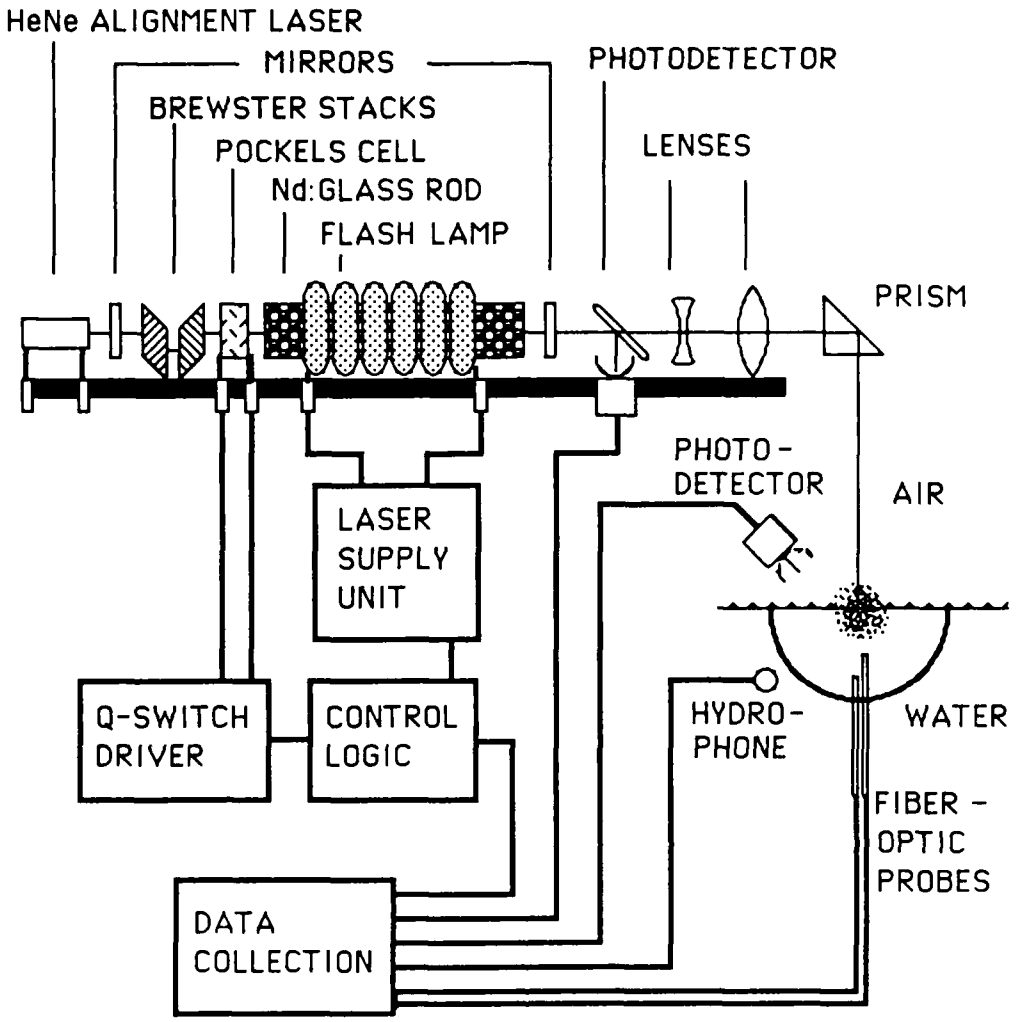

FIGURE 17

SCHEMATIC OF THE IMPROVED EXPERIMENTAL APPARATUS

AS-86-491

the blast process and, with the acoustic sensors, their contributions to the acoustic output. The process is expected to be complicated by oscillations of the gas bubble, which is formed as a by-product of the blast. When the process is understood with sufficient precision, it would be possible to make estimates of its optoacoustic energy conversion efficiency, particularly in the band of useful sonar frequencies.

APPENDIX A
HYDROPHONE CALIBRATIONS

Calibration charts for the three hydrophones used in our experiment, the E8-59, E8-62, and H23, are shown in Figs. A-1 through A-3. The H23 was calibrated for the band 1 kHz to 150 kHz, the E8-59 was calibrated from 100 kHz to 1 MHz, and the E8-62 from 200 kHz to 1 MHz. These charts were made by Naval Research Laboratory, Orlando, Florida. Although the calibration chart for the E8-62 only extends to 200 kHz, we were able to estimate its calibration down to 100 kHz by comparing the broadband response of the E8-62 to that of the E8-59. Between 200 kHz and 600 kHz the responses of these two hydrophones are almost the same, and therefore we were able to get a relative calibration of the E8-62 by taking the Fourier transforms of their responses to two identical broadband signals which had the same levels beyond 200 kHz and then dividing the response of the E8-62 response by that of the E8-59 for frequencies between 100 kHz and 200 kHz. The hydrophones are shown in Figs. A-4 and A-5. The dotted regions represent the active elements.

COURTESY OF NAVAL
RESEARCH LABORATORY/UNDERWATER
SOUND REFERENCE DIVISION

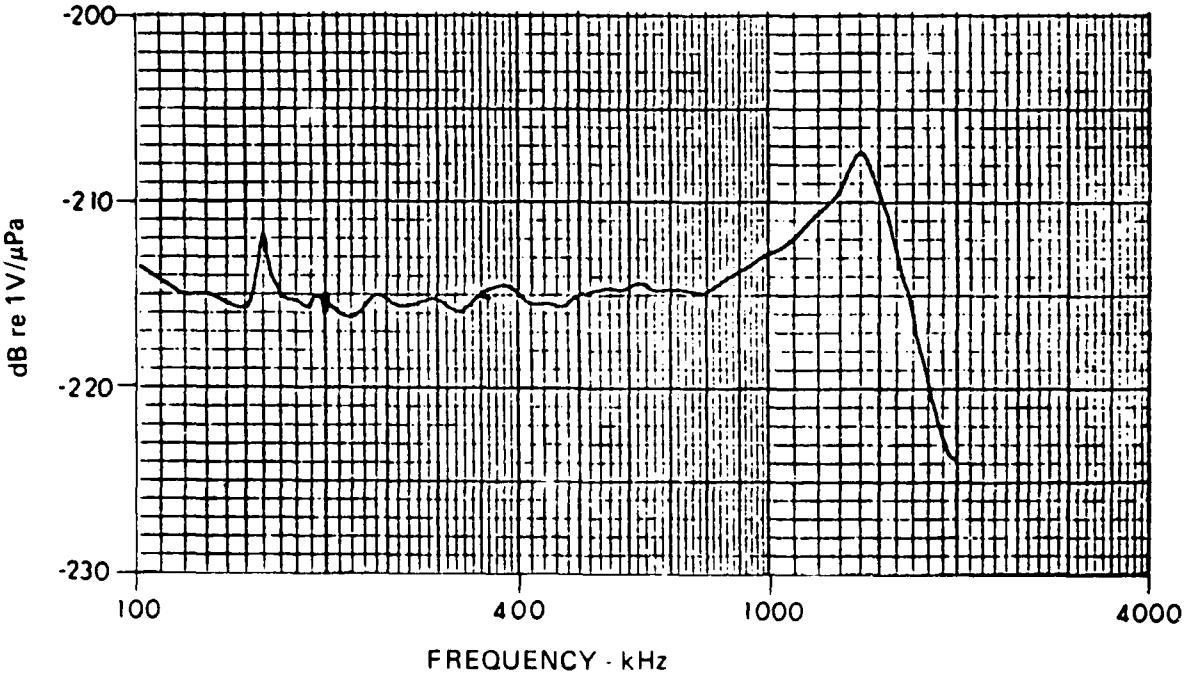

FIGURE A-1
CALIBRATION CURVE OF THE E8-59 HYDROPHONE

ARL UT
AS - 86 - 118
NPC - GA
3 - 28 - 86

COURTESY OF NAVAL
RESEARCH LABORATORY/UNDERWATER
SOUND REFERENCE DIVISION

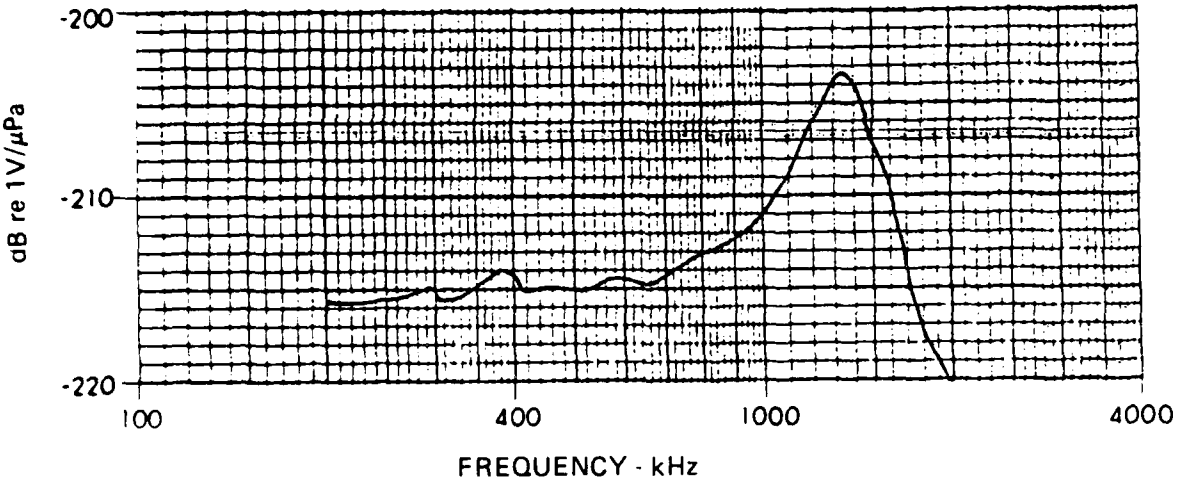

FIGURE A-2
CALIBRATION CURVE OF THE E8-62 HYDROPHONE

ARL UT
AS-86-119
NPC-GA
3-28-86

COURTESY OF NAVAL
RESEARCH LABORATORY/UNDERWATER
SOUND REFERENCE DIVISION

HYDROPHONE VOLTAGE COUPLING GAIN (RATIO
IN dB OF VOLTAGE AT PREAMPLIFIER OUTPUT TO
OPEN CIRCUIT CRYSTAL VOLTAGE): 0.1 to 100 kHz = 8.9 dB
150 kHz = 9.2 dB

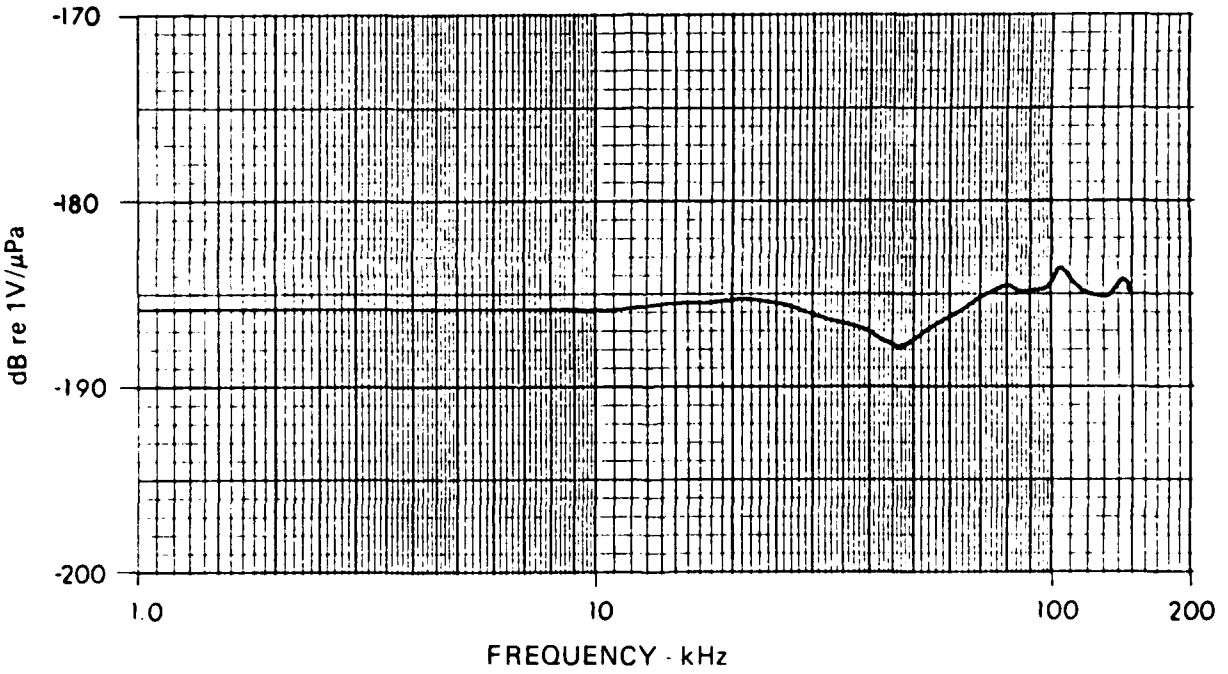

FIGURE A-3
CALIBRATION CURVE OF THE H23 HYDROPHONE

ARL:UT
AS-86-117
NPC-GA
3-28-86

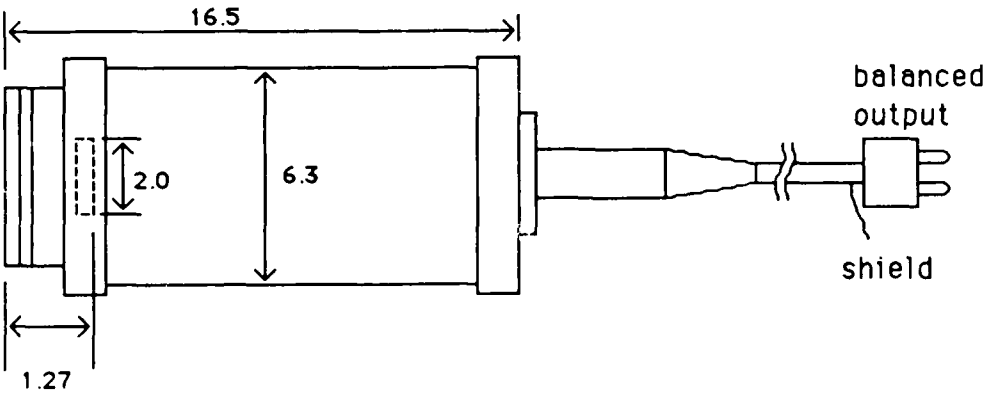

FIGURE A-4

THE E8 HYDROPHONE: DIMENSIONS IN CENTIMETERS
The dotted area indicates the acoustically active region

AS-86-492

APPENDIX B
Q-SWITCH DRIVER CONTROL CIRCUIT

The Q-switch driver control circuit is a TTL circuit designed to send a series of trigger pulses to the Q-switch driver. It can be set to send a designated number of pulses with a particular repetition rate after a preset delay. The control circuit has four sections to it as shown in Fig. B-1. The first section buffers the trigger pulse from the laser firing unit and provides a clean trigger pulse to the state graph controller. This section is necessary because the laser will often send two or more trigger pulses. The second section is the state graph which controls the sequencing of events. The third section is the timing section, which defines the number of pulses, the repetition rate, and the initial delay. The fourth section, a clock, provides the timing for the state graph.

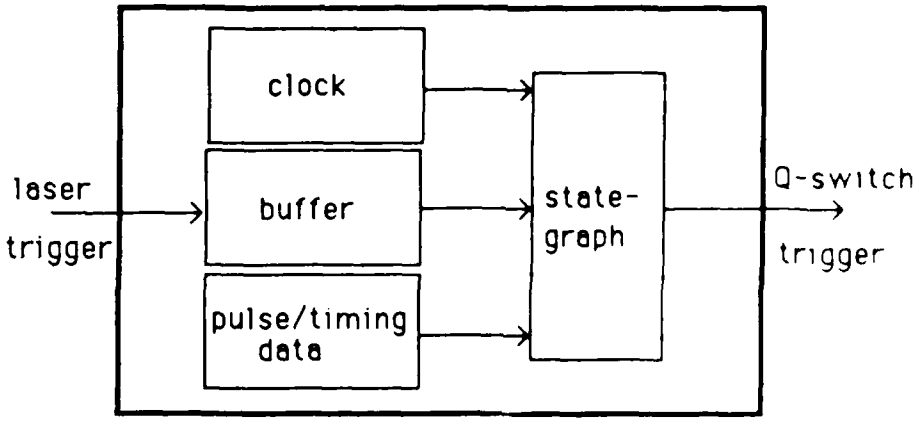

FIGURE B-1

SCHEMATIC OF THE Q-SWITCH DRIVER CONTROL CIRCUIT

APPENDIX C
DETERMINATION OF SOURCE WIDTH AND DEPTH

At any given frequency, the discrepancy between the acoustic signal level produced by a distributed source and a point source of equal power is termed a "diffraction loss." For a white noise source, diffraction losses, resulting from the finite dimensions of the source volume, will impose an upper cutoff frequency on the acoustic signal. At frequencies above the cutoff, significant diffraction loss is incurred due to the destructive interference of signal elements from spatially separate points within the source volume. Conversely, if the cutoff frequency is observable then it is possible to make estimates of the physical dimensions of the source volume. The cutoff occurs at the frequency where the acoustic wavelength is approximately equal to the projected length of the source in the direction of the observer. The exact cutoff frequency and the spectral response is dependent on the details of the source density function within the source volume. Nevertheless, it is possible to get an approximate estimate of the source volume dimensions by approximating the source density with an idealized standard function such as a Gaussian or an exponential function. The relationship between the source dimensions and the cutoff frequency for a few idealized source density functions are derived below.

[illegible] source volume is assumed to be disk shaped, where the width [illegible] the depth. The width of the optoacoustic source, as generated [illegible] may be estimated from the upper cutoff frequency of the acoustic [illegible] signal in the horizontal direction, where the projected width D' is equal [illegible] multiplied by $\sin\theta_0$, as shown in Fig. C.1. This is an [illegible] based assumption that the distance to the receiver is very [illegible] We used a value of 45° for θ_0 in our experimental [illegible] estimate the depth, of the source volume, we would [illegible] below the blast, where only the depth [illegible]

[illegible] is necessary to assume [illegible] and experimental

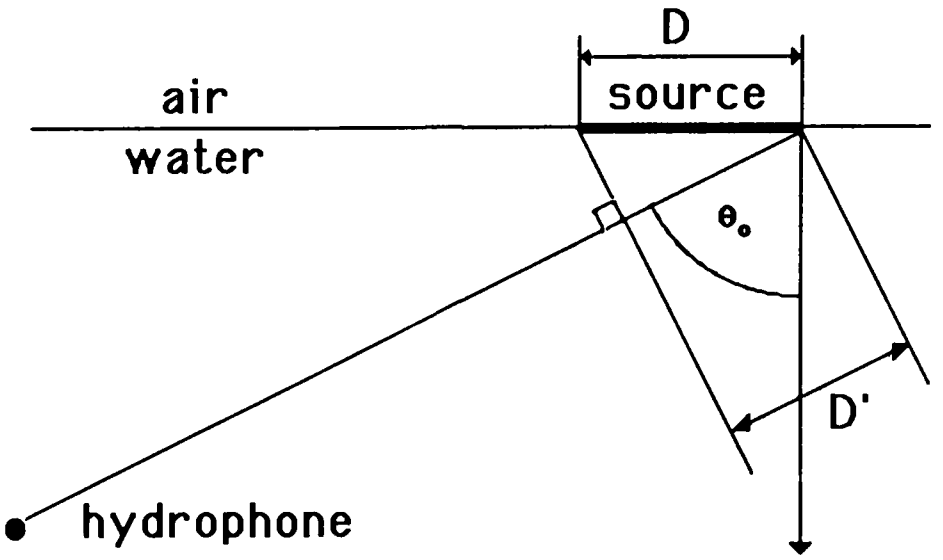

FIGURE C-1

DIFFRACTION LOSS GEOMETRY

AS-86-495

A. The Uniform Density Function

Assuming a uniform surface source density function, the diffraction loss factor D_a is given by

$$D_a = \int_{x=-r}^{x=r} (\pi r^2)^{-1} \; 2\sqrt{(r^2 - x^2)} \cos((x/\lambda)\, 2\pi \sin\theta_0)\, dx \quad , \qquad (C.1)$$

where r is the radius of the blast aperture, θ_0 is the angle to the receiver referenced to the downward vertical, and λ is the wavelength corresponding to the cutoff frequency. Using the substitution, $u = x/r$, $du = dx/r$, Eq. (C.1) becomes

$$D_a = \int_{-1}^{1} (\pi r^2)^{-1} \; 2r\sqrt{(1 - u^2)} \cos((ur/\lambda)\, 2\pi \sin\theta_0)\, (r du) \quad . \qquad (C.2)$$

Simplifying Eq. (C.2) and taking advantage of the function's symmetry about the origin gives

$$D_a = \int_{0}^{1} (4/\pi)\sqrt{(1 - u^2)} \cos(u 2\pi r \sin\theta_0/\lambda)\, du \quad . \qquad (C.3)$$

The solution is expressible as a Bessel function,

$$D_a = (\lambda/(\pi r \sin\theta_0))\; J_1(2\pi r \sin\theta_0/\lambda) \quad , \qquad (C.4)$$

where J_1 is a first order Bessel function. By substituting the wavelength λ with the -3 dB cutoff wavelength λ_c which is related to the cutoff frequency f_c by

$$\lambda_c = c/(2\pi f_c) \quad , \qquad (C.5)$$

where c is the speed of sound in water, and setting D_a equal to $(1/\sqrt{2})$, an expression for the radius r of may be found.

B. The Gaussian Density Function

A Gaussian function is another plausible approximation for the surface source distribution. The equation is

$$D_a = (\pi a^2)^{-1} \int_{-\infty}^{\infty} \int_{-\infty}^{\infty} \exp[-(x^2 + y^2)/a^2] \cos(x2\pi \sin\theta_0 / \lambda)\, dx\, dy \quad , \qquad (C.6)$$

where a is the 1/e radius of the blast aperture. The integration with respect to x gives

$$D_a = 2 (\sqrt{\pi a^2})^{-1} \int_0^{\infty} \exp[-(a\pi \sin\theta_0 / \lambda)^2] \int \exp[-y^2/a^2]\, dy \quad . \qquad (C.7)$$

Integrating with respect to y and simplifying gives

$$D_a = \exp[-(a\pi \sin\theta_0 / \lambda)^2] \quad . \qquad (C.8)$$

Setting D_a equal to $1/\sqrt{2}$, λ to λ_c, and solving for a gives

$$a = \sqrt{(\ln 2/2)}\ \lambda_c / (\pi \sin\theta_0) \quad . \qquad (C.9)$$

C. The Exponential Density Function

The exponential density model is a plausible approximation for the vertical source density. The diffraction loss for the θ_0=0 case is given by

$$D_a = a^{-1} \int_0^{\infty} \exp[-z/a] \exp[j2\pi z/\lambda]\, dz\, |^2 \qquad (C.10)$$

The solution is simply

$$D_a = \lambda^2 / (\lambda^2 + 4\pi^2 a^2) \qquad (C.11)$$

Setting D_a equal to $1/\sqrt{2}$, λ to λ_c, and solving for a gives

$$a = \lambda/2\pi \quad . \tag{C.12}$$

D. Estimates of Width and Depth of the Optoacoustic Source

Estimates of width and depth estimates based on data at $\theta_o = 45°$ and $\theta_o = 0°$ obtained from the three different models of source density are given in Table C-1.

TABLE C-1
ESTIMATED DIMENSIONS OF OPTOACOUSTIC SOURCE

density function	width (mm)	depth (mm)
uniform	1.08	N/A
Gaussian	0.72	N/A
exponential	N/A	0.084

REFERENCES

1. N. P. Chotiros, "The Moving Thermoacoustic Array: A Theoretical Feasibility Study," Applied Research Laboratories Technical Report No. 85-3 (ARL-TR-85-3), Applied Research Laboratories, The University of Texas at Austin, 1985.

2. L. M. Lyamshev and K. A. Naugolnikh, "Optical Generation of Sound : Nonlinear Effects (Review)," Sov. Phys.-Acoust. 27(5) (1981).

3. T. G. Muir, C. R. Culbertson, and J. R. Clynch, "Experiments on Thermoacoustic Arrays with Laser Excitation," J. Acoust. Soc. Am. 59, 735-743 (1976).

4. M. W. Sigrist and F. K. Kneubuhl, "Laser-Generated Stress Waves in Liquids," J. Acoust. Soc. Am. 64(6), 1652-1663 (1978).

5. B. S. Maccabee and C. E. Bell, "Acoustic Pressure Scaling of Laser Induced Sound," NSWC TR 82-122, Naval Surface Weapons Center, Silver Spring Maryland, 1982.

6. D. C. Emmony, B. M. Geerken, and A. Straaijer, "The Interaction of 10.6 μm Laser Radiation with Liquids," Infrared Physics 16, 87-92 (1976).

7. E. F. Carome, C. E. Moeller, and N. A. Clark, "Intense Ruby-Laser-Induced Acoustic Impulses in Liquids," J. Acoust. Soc. Am. 40(6) 1462-1466 (1966).

8. G. D. Hickman and J. A. Edmonds, "Laser-Acoustic Measurement for Remotely Determining Bathymetry in Shallow Turbid Waters," J. Acoust. Soc. Am. 73(3),840-843 (1983).

9. C. E. Bell and B. S. Maccabee, "Shock Wave Generation in Air and Water by CO_2 TEA Laser Radiation," Applied Optics 13(3), 605-609 (1974).

10. B. S. Maccabee and C. E. Bell, NSWC TR 83-13C, Naval Surface Weapons Center, Silver Spring, Maryland, 1983.

11. B. S. Maccabee and C. E. Bell, "Experimental Study of Laser-Induced Underwater Sound." J. Acoust. Soc. Am. 77, S103 (1985).

12. A. N. Pirri, R. Schier, and D. Northam, "Momentum Transfer and Plasma Formation above a Surface with a High-Power Laser," Appl. Phys. Lett., 21(3) 79-81 (1972).

13. A. N. Pirri, "Theory for Momentum Transfer to a Surface with a High-Power Laser," Phys. Fluids 16,1435 (1973).

14. P. K. Wu, "Radiation Induced Acoustic Waves in Water," AIAA Journal 15(12) 1809-1811 (1977).

15. Yu. P. Raizer, "Heating of a Gas by a Powerful Laser Light," Soviet Physics JETP 21(5) 1009-1017 (1965).

16. L. I. Sedov, Similarity and Dimensional Methods in Mechanics (Academic Press, New York, 1959), pp. 220.

17. M. Schulkin and H. W. Marsh, "Absorption of Sound in Sea Water," J. Brit. IRE 25, 493 (1963). Also, "Sound Absorption in Sea Water," J. Acoust. Soc. Am. 34, 864 (1962).

18. R. M. Hall and M. Holt, "Numerical Solutions of the Upper Critical Depth Problem," AIAA J. 14, 191-198 (1976).

12 August 1986

DISTRIBUTION LIST FOR
ARL-TR-86-11
UNDER CONTRACT N00014-86-K-0176

Copy No.	
	Office of Naval Research Department of the Navy Arlington, VA 22217
1	Attn: R. Fitzgerald (Code 1125UA)
2	R. Obrochta (Code 1125AR)
	Director Naval Research Laboratory 455 Overlook Ave., S.W. Washington, DC 20375
3	Attn: Code 2627
4 - 15	Commanding Officer and Director Defense Technical Information Center Bldg. 5, Cameron Station Alexandria, VA 22314
	Naval Surface Weapons Center White Oak Laboratory Silver Spring, MD 20910
16	Attn: C. Bell
	School of Mechanical Engineering Georgia Institute of Technology Atlanta, GA 30332
17	Attn: A. Pierce
18	P. Rogers
19	Y. Berthelot
	Mechanical Engineering Department The University of Texas at Austin Austin, TX 78713
20	Attn: D. Wilson
	Electrical Engineering Department The University of Texas at Austin Austin, TX 78713
21	Attn: M. Becker
22	Advanced Sonar Group, ARL:UT

Distribution List for ARL-TR-86-11 under Contract N00014-86-K-0176 (cont'd)

Copy No.	
22	David T. Blackstock, ARL:UT
23	Nicholas P. Chotiros, ARL:UT
24	C. Robert Culbertson, ARL:UT
25	Reuben H. Wallace, ARL:UT
26 - 36	Library, ARL:UT

END

2-87

DTIC